

On Transmission–Zeros of Piezoelectric Structures

Shashank Pathak¹, Dimitri Piron^{1,2}, Ahmad Paknejad^{1,2}, Christophe Collette^{1,2}, and Arnaud Deraemaeker^{1,3}

¹Precision Mechatronics Laboratory (PML), Université Libre de Bruxelles, Brussels, Belgium

²Precision Mechatronics Laboratory (PML), Université de Liège, Liège, Belgium

³Building Architecture and Town Planning (BATir), Université libre de Bruxelles, Brussels, Belgium

Abstract

The evaluation of transmission zeros is of great importance for the control engineering applications. The structures equipped with piezoelectric patches are complex to model and usually require finite element approaches supplemented by model reduction. This study rigorously investigates the influence of mesh size, model reduction, boundary conditions (free and clamped), and sensor/actuator configuration (collocated and non-collocated) on the evaluation of transmission zeros of the piezoelectric structures. The numerical illustrations are presented for a thin rectangular plate equipped with a single pair of piezoelectric voltage sensor/ voltage actuator. Through the examples considered in this study, a link is presented between the static response (or static deflected shape) and the transmission zeros of the piezoelectric structures. This interesting observation forms the basis of: (i) a local mesh refinement strategy for computationally efficient estimation of the transmission zeros and (ii) a physical interpretation of the pole-zero pattern in the case of piezoelectric structures. The physical interpretation developed in this study helps in qualitatively explaining the pole-zero patterns observed for different configurations. It is also shown that this understanding of the relation between the static deformed shape and the transmission zeros can be used by the practitioners to modify the pole-zero pattern through a careful selection of the orientation and the size of the piezoelectric patches.

Keywords: Piezoelectric patches, Transmission zeros, Static response, Physical interpretation,

Pole-zero pattern.

1 Introduction

The transmission zeros play a major role in active vibration control and need to be determined precisely in order to assess the performance of the active vibration control strategies (Preumont, 2018). Therefore, (i) an efficient and accurate computation of the zero frequencies, (ii) the parameters influencing their values, and (iii) their physical interpretation are of great interest in control engineering research.

Unlike poles of a system which represent the vibration modes of the structure, the transmission zeros are not the fundamental characteristics of a structure. In fact, their values depend upon the type the sensors and actuators (e.g., force-displacement pair, piezoelectric patches, etc.) and their configuration (collocated or non-collocated). The transmission zeros can be evaluated using different approaches such as the constrained mode theory (Williams, 1992a), the state-space approach (Wolovich, 1973; Davison & Wang, 1974; Emami-Naeini & Van Dooren, 1982), or an analytical approximation based on nearby modeshapes (Piron et al., 2021). The determination of transmission zeros of large and complex structures usually requires finite element modelling (FEM) supplemented by model reduction in the bandwidth of interest which truncates the higher frequency modes. The truncation of higher frequency dynamics leads to: (i) the overestimation of the transmission zeros of a collocated force-displacement sensor/actuator (SA) pair (Williams, 1992b), whereas in the case of a non-collocated SA pair there is no definite trend (Allen & Lauffer, 1992), (ii) the radical changes in pole-zero pattern especially for the structures with non-collocated SA pair(s) and with distributed sensors and actuators (such as piezoelectric transducers) (Lindner et al., 1993), and (iii) the erroneous non-minimum phase zeros in some cases of the non-collocated SA pair(s) depending on the mesh size and the SA separation (Henrich et al., 1994). The research efforts accounting for this truncation error have shown that: (i) in the case of collocated SA pair(s), the transmission zeros converge monotonically with increasing model order with a higher convergence rate for lower order zeros while the monotonic convergence of the zeros is not guaranteed for the non-collocated SA pair(s) (Williams, 1992b), on the other hand, (ii) the accuracy of the zeros may be enhanced further by

including the static deflection information (static correction) and/or higher order interpolation functions (in FEM) without increasing the model order (Fleming, 1990; Fleming & Crawley, 1991).

For successful implementation of optimal control strategies, the previous research efforts also attempted to understand the properties and behaviour of transmission zeros (Williams, 1989; Spector & Flashner, 1990; Fleming, 1990; Fleming & Crawley, 1991; Williams, 1992c). These studies highlighted: (i) the interlacing property of the poles and zeros of the structures equipped with collocated SA pair(s) and the dependence of the zeros on SA placement, (ii) the disappearance of the alternating pole-zero pattern for non-collocated SA pair(s), (iii) the higher sensitivity of zeros to the location of collocated dual SA pair(s) in higher modes and for highly constrained systems, (iv) the insensitivity of the zeros in the case of collocated SA pair(s) located in the vicinity of a node and a finite sensitivity for non-collocated and/or non-dual SA pair(s), and (v) the high sensitivity of the zeros of non-collocated systems to the modelling errors and SA locations which may also result in pole-zero flipping.

The physical interpretation of transmission zeros is very well understood based on the resonances of the constrained subsystems of the flexible structures with collocated dual SA pair(s) for single-input-single-output (SISO) systems (Miu, 1991; Williams, 1992a), for multi-input-multi-output (MIMO) systems (Bona et al., 1996; Calafiore et al., 1997; Preumont et al., 2008), and for MIMO mass-dashpot-spring systems with non-collocated SA pair(s) (Lin, 1999). Calafiore (1997) identified that the zero modes are closely related to the energetically isolated subsystems of the original system in the case of linear MIMO flexible mechanical systems. Another well-known interpretation is based on energy flow within a physical subsystem and is described using the bond graph representation (Van de Straete, 1995; Van de Straete & Youcef-Toumi, 1996).

However, the aforementioned studies are mainly applicable to the force-displacement SA pair(s) and may only be indicative in the case of structures equipped with piezoelectric SA patches. The piezoelectric materials are frequently used as distributed actuators and sensors in vibration control applications (e.g. Rao & Sunar, 1994; Balamurugan & Narayanan, 2001; Moheimani & Fleming, 2006; Sharma et al., 2020) and a detailed review of piezoelectric-based

structural control techniques and strategies can be referred from [Chee et al. \(1998\)](#); [Song et al. \(2006\)](#); [Iorga et al. \(2008\)](#); [Gupta et al. \(2010\)](#); [Qureshi et al. \(2014\)](#); [Gripp and Rade \(2018\)](#); [Shivashankar and Gopalakrishnan \(2020\)](#). Most of the research efforts, related to the piezoelectric structures, have been directed towards: (i) minimizing the effect of the modal truncation on dynamics in the bandwidth of interest ([Moheimani, 1999](#); [Moheimani & Clark, 2000](#)), (ii) developing efficient finite element modelling techniques and tools for piezoelectric structures ([Piefort, 2001](#); [Xu & Koko, 2004](#); [Spier et al., 2011](#); [Balmes & Deraemaeker, 2013](#); [Bendine et al., 2017](#)), (iii) the optimization of control architecture of piezoelectric sensors and actuators (e.g. [Halim & Moheimani, 2003](#); [Gupta et al., 2010](#); [Bendine et al., 2019](#)), and (iv) vibration control using the shunted piezoelectric transducers (e.g. [Gripp & Rade, 2018](#)), the active control (e.g. [Takács et al., 2012](#); [Moghaddam & Ahmadi, 2020](#)), and the hybrid control (e.g. [Tang & Wang, 2001](#)). Some notable efforts are also made towards improving the understanding of the dynamics of piezoelectric structures. For example, based on a comparison between analytical and experimental dynamic response of a simply supported beam excited by distributed multiple piezoelectric actuators, [Clark et al. \(1991\)](#) concluded that one dimensional models ignore the increase in beam stiffness due to the strain generated in the transverse direction and suggested to use the two dimensional models for higher accuracy. Later, [Qing et al. \(2006\)](#) improved the accuracy further by including transverse shear deformation and the rotary inertia in the FEM of piezoelectric plates.

In addition to the above, a few fundamental and conceptual studies can also be found but those are limited to: (i) the classical collocated systems with actuating and sensing layers entirely covering both sides of the beam demonstrating alternating poles and zeros ([Alberts & Colvin, 1991](#); [Cudney et al., 1992](#)), and (ii) considering only a certain type of non-collocation where only the sizes of the actuator and sensor patches are different while their centroids are collocated ([McCain, 1995](#); [Andersson & Crawley, 1996](#)). Moreover, there is no dedicated study to understand the physical interpretation of the transmission zeros of piezoelectric structures and a possible reason may be the fact there are several complications associated with the modelling and the physical understanding of such structures. For example, unlike force-displacement SA pairs, in the case of piezoelectric patches, the actuation and sensing mechanisms are linked

to the average strains measured over the area of the patch and the applied boundary forces which makes the dynamics quite complicated (e.g. [Tondreau et al., 2014](#)). Furthermore, the piezoelectric patches are never truly collocated except when the same transducer is used for actuation as well as sensing ([Dosch et al., 1992](#)). Also, [Piefort and Preumont \(2001\)](#) discussed that the local effects such as membrane strains (in thin shells) play a crucial role in affecting the transmission zeros of piezoelectric shell structures.

The state-of-the-art presented above highlights the fact that while many studies have focused on different aspects of modeling to predict transmission zeros accurately in piezoelectric structures, there has not been an attempt to give a physical interpretation to them. Such an interpretation is straightforward for force-displacement SA pairs where the zeros correspond to natural frequencies of the structure constrained at the location and in the direction of the SA pair, but cannot be extended to piezoelectric structures due to the fact that SA pairs are rarely strictly collocated. The interpretation presented in this paper is based on the understanding of the importance of static correction to model accurately the zeros, which links the zeros to the static response of the system. The originality of the work is to use the link between the static correction and the static response to give a physical interpretation to the zeros by looking at the relative importance between the contribution of the low frequency modes and this static deflection. The influence of different parameters such as the dimension and orientation of the patches, as well as the boundary conditions can be understood physically by looking at these different contributions, which allows to better understand the potential optimal configurations for control applications.

The current paper is organized as follows: (i) Section 2 introduces the general finite element formulation of the piezoelectric structures followed by a discussion on model reduction and static correction, (ii) Section 3 presents the different finite element models used in this study, (iii) Section 4 and (iv) Section 5, respectively, discuss the influence of modal truncation and mesh size on the evaluation of the transmission zeros which eventually highlights a link between the static response and the transmission zeros, (v) Considering this link, a physical interpretation is proposed for the pole-zero pattern in Section 6, and (vi) Section 7 summarizes the key points and contributions of this paper.

2 Finite Element Formulation

The structures equipped with piezoelectric voltage actuators and piezoelectric voltage sensors can be modelled as laminated finite element shell or solid elements depending on the modelling requirements. The strains generated in the structure can be attributed to the four main components: (i) membrane strain, (ii) curvature strain, (iii) transverse shear strain, and (iv) electric field. It is assumed for the laminated shells, which will be used in this study, that: (i) the polarization of piezoelectric patches is such that a uniform electric field is produced only along the thickness of the patches and (ii) the principal axes of the patches are parallel to the structural orthotropy axes. The generalized constitutive equations of a piezoelectric structure can be written using the Hamilton's principle in the matrix form as (Yang, 2005):

$$\begin{bmatrix} M_{uu} & 0 & 0 \\ 0 & 0 & 0 \\ 0 & 0 & 0 \end{bmatrix} \begin{Bmatrix} \ddot{U} \\ \ddot{V}_s \\ \ddot{V}_a \end{Bmatrix} + \begin{bmatrix} K_{uu} & K_{uv_s} & K_{uv_a} \\ K_{v_s u} & K_{v_s v_s} & 0 \\ K_{v_a u} & 0 & K_{v_a v_a} \end{bmatrix} \begin{Bmatrix} U \\ V_s \\ V_a \end{Bmatrix} = \begin{Bmatrix} F \\ Q_s \\ Q_a \end{Bmatrix} \quad (1)$$

where, (i) vector $\{U\}_{N_m \times 1}$ contains N_m mechanical (displacements and rotations) degrees of freedom (DOFs), (ii) vectors $\{V_s\}_{N_s \times 1}$ (N_s = number of sensor patches) and $\{V_a\}_{N_a \times 1}$ (N_a = number of actuator patches) represent the electric DOFs (voltages or potential difference) across the electrodes of the sensor and actuator patches, respectively, (iii) vector $\{F\}_{N_m \times 1}$ consists of external mechanical forces, (iv) vectors $\{Q_s\}_{N_s \times 1}$ and $\{Q_a\}_{N_a \times 1}$ represent the charge accumulated on sensor electrodes and the charge imposed on actuator electrodes, respectively, (v) M_{uu} is the $N_m \times N_m$ mass matrix corresponding to the mechanical DOFs, (vi) K_{uu} is the $N_m \times N_m$ stiffness matrix corresponding to the mechanical DOFs, (vii) $K_{uv_s [N_m \times N_s]} = K^T_{v_s u [N_s \times N_m]}$ and $K_{uv_a [N_m \times N_a]} = K^T_{v_a u [N_a \times N_m]}$ are piezoelectric coupling matrices, and (viii)

the submatrix $\begin{bmatrix} K_{v_s v_s} & 0 \\ 0 & K_{v_a v_a} \end{bmatrix}_{(N_s+N_a) \times (N_s+N_a)}$ represents the capacitance matrix.

The generalized constitutive equation (Eq. 1) can be simplified based on the choice of voltage and/or charge sensor and/or actuator. In the current study, we have mainly used the

voltage actuator (i.e., short circuit condition at the actuator patches and $F = 0$) and the voltage sensor (open circuit condition at the sensor patches, i.e, $Q_s = 0$), therefore, Eq. 1 can be simplified as the following two equations:

$$\begin{bmatrix} M_{uu} & 0 \\ 0 & 0 \end{bmatrix} \ddot{U}_{eq} + \begin{bmatrix} K_{uu} & K_{uv_s} \\ K_{v_s u} & K_{v_s v_s} \end{bmatrix} U_{eq} = F_{eq} \quad (2)$$

$$Q_a = K_{v_a u} U + K_{v_a v_a} V_a \quad (3)$$

where $U_{eq} = [U \quad V_s]^T$, $F_{eq} = -[K_{uv_a} V_a \quad 0]^T$, and Eq. 3 relates the charges Q_a (on the actuator patches) to the enforced voltages V_a (on the actuator patches).

The electromechanical analogy between mechanical displacement and electric voltage allows to treat the voltage DOFs just like the displacement DOFs (Piefort, 2001) and leads to the modal decomposition of Eq. 2 by changing the physical coordinates (U_{eq}) to the modal coordinates (X) as:

$$U_{eq} = [\phi] \{X\} \quad (4)$$

where $[\phi]$ is the matrix containing $N_m + N_s$ mode shapes (eigenvectors) which can be obtained by solving the following eigenvalue problem:

$$\left(\begin{bmatrix} K_{uu} & K_{uv_s} \\ K_{v_s u} & K_{v_s v_s} \end{bmatrix} - \omega_i^2 \begin{bmatrix} M_{uu} & 0 \\ 0 & 0 \end{bmatrix} \right) \{\phi_i\} = 0 \quad (5)$$

where $\{\phi_i\}$ is the i^{th} eigenvector in the matrix ϕ and ω_i is the corresponding eigenfrequency such that $i = 1, \dots, N_m + N_s$. Substituting Eq. 4 in Eq. 2 and applying the orthogonality properties of eigenvectors (w.r.t. mass and stiffness matrices) leads to the following uncoupled equations:

$$\mu \ddot{X} + \mu \Omega^2 X = \phi^T F_{eq} \quad (6)$$

where $\mu = \text{diag}(\mu_i) = \phi^T \begin{bmatrix} M_{uu} & 0 \\ 0 & 0 \end{bmatrix} \phi$ and $\mu \Omega^2 = \text{diag}(\mu_i \omega_i^2) = \phi^T \begin{bmatrix} K_{uu} & K_{uv_s} \\ K_{v_s u} & K_{v_s v_s} \end{bmatrix} \phi$. The

uncoupled Eqs. 6 can be used to obtain the transfer function or the frequency response function (FRF) $G_{as}(\omega)$ between the a^{th} voltage actuator and the s^{th} voltage sensor as follows:

$$G_{as}(\omega) = \sum_{i=1}^{N_m+N_s} \frac{b_s \phi_i \phi_i^T b_a}{\mu_i(\omega_i^2 - \omega^2)} \quad (7)$$

where $\{b_s\} = \{\{0\}_{1 \times (N_m+s-1)} \quad 1 \quad \{0\}_{1 \times (N_s-s)}\}^T$ and $\{b_a\} = -\{\{K_{uvaa}\}^T \quad \{0\}_{1 \times N_s}\}^T$ are $(N_m + N_s) \times 1$ influence vectors such that $\{K_{uvaa}\} = a^{th}$ column of the matrix K_{uva} .

2.1 Ideally- and nearly-collocated configurations

The above formulation can be similarly extended to the other choices (voltage or charge) of the sensors and actuators. It is also to be noted that it can take into account collocated as well as non-collocated configurations. There are two possibilities of collocated configurations of the piezoelectric SA patches as shown in Fig. 1. The first one is the case of real collocation when the same piezoelectric patch is used for sensing as well as actuation and the second one is the case of near-collocation when the actuator and sensor patches are at the same location but on opposite sides of the structure (with coinciding centroids of the patches).

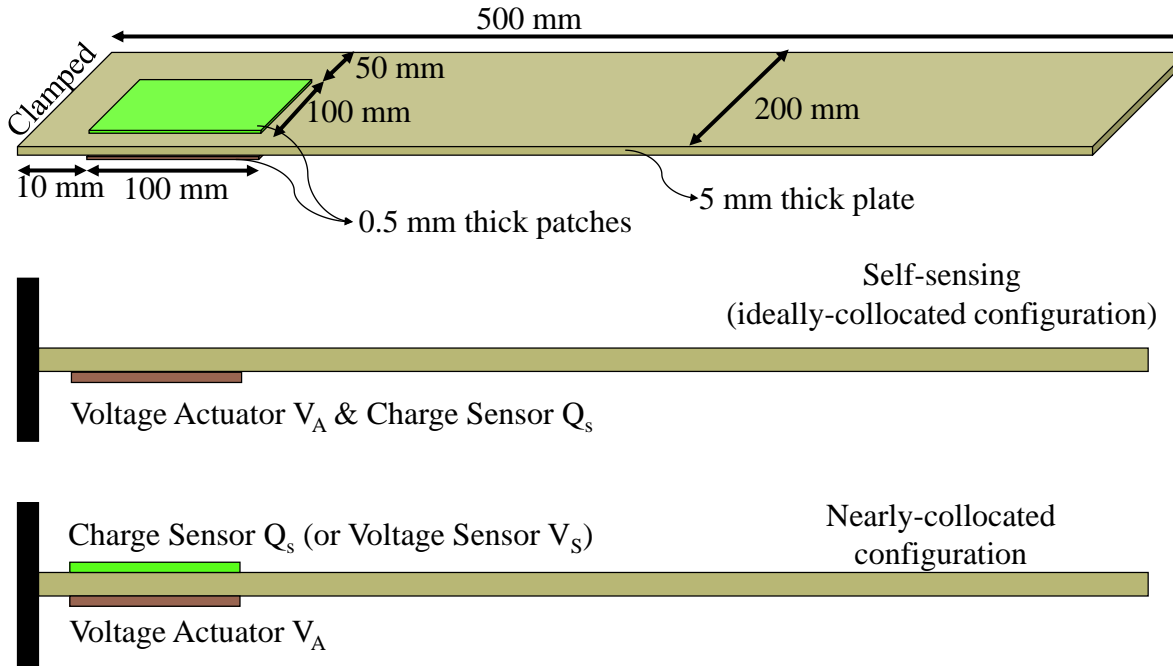
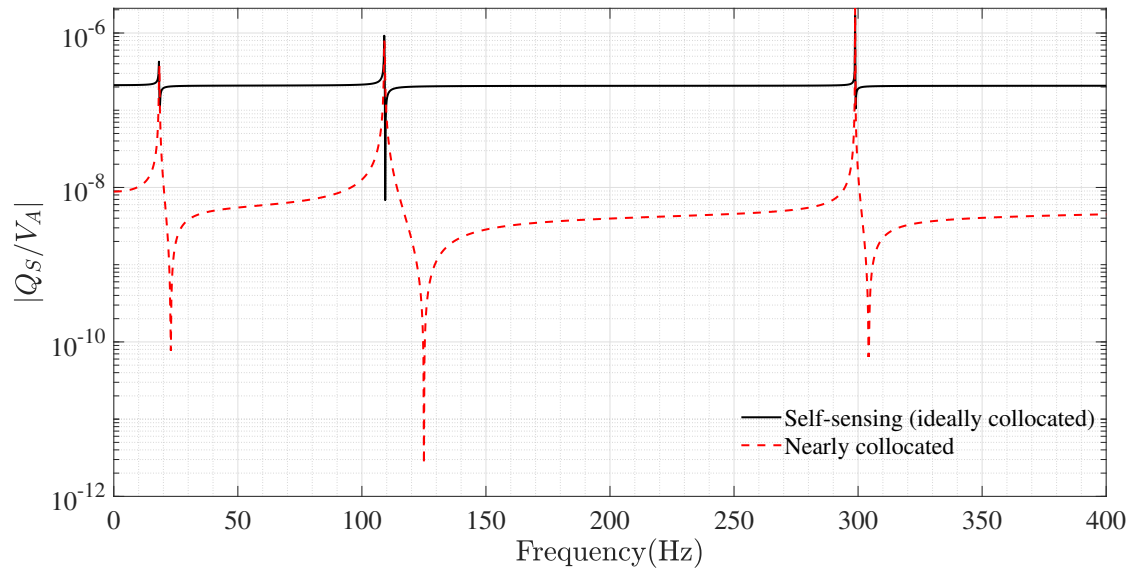


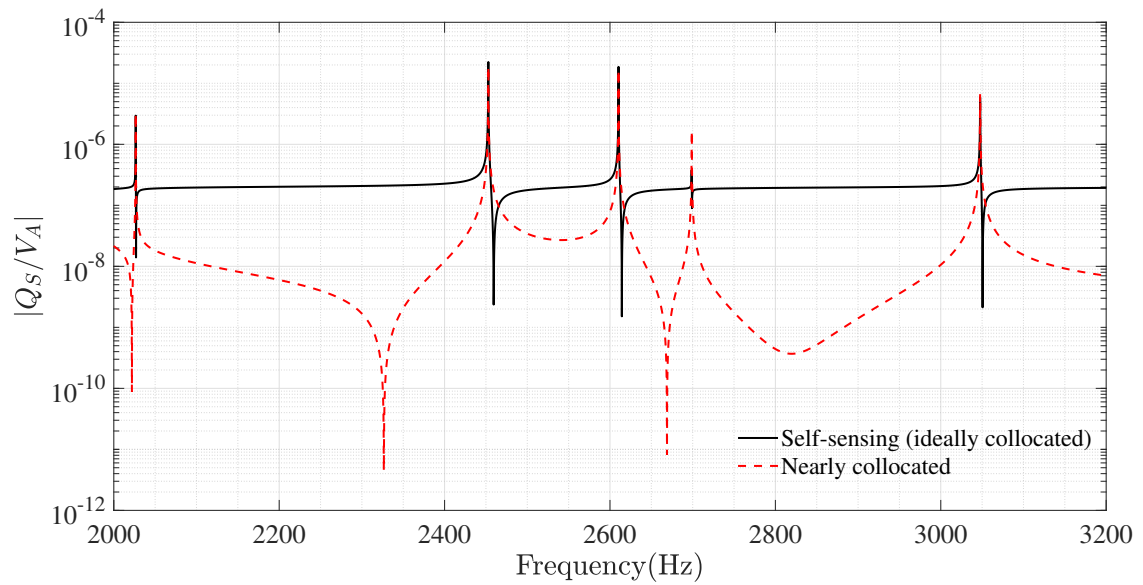
Fig. 1. A pictorial representation of nearly- and real-collocated configurations of a cantilever plate equipped with piezoelectric SA patches

To compare these two types of (collocated) configurations, the example of an aluminium cantilever plate equipped with nearly-collocated and ideally-collocated piezoelectric patches is considered as shown in Fig. 1. For the purpose of illustration, in both cases a voltage actuator (V_A) is used. Because, the ideally-collocated system can have only charge sensor (Q_S) in the case of voltage actuation, therefore, the FRF between the voltage actuator and charge sensor are compared for the two configurations as shown in Fig. 2. The respective FRFs are obtained through finite element modelling and analysis. The details required for the FEM such as material and element properties will be discussed later in the Section 3.

As expected, the self-sensing configuration exhibits interlaced pole-zero pattern at all the frequencies, whereas the nearly-collocated configuration loses the alternating pole-zero pattern at frequencies higher than 2000 Hz. The distances between the poles and zeros of the self-sensing configuration are very small compared to the nearly-collocated configuration. A common example of the use of strictly collocated configuration is the passive resistive or RL shunts. In this case, it is well known that the amount of damping that can be added to the structure is proportional to the distance between the poles and zeros. The efficiency of such devices is therefore limited, and this is the main reason for adopting nearly collocated configurations for active vibration damping applications. In view of this, the current study investigates only nearly-collocated configuration which will be referred hereafter as ‘collocated’ configuration. In the case of self-sensing, the transmission zeros can be interpreted as the poles of the open circuit system (Preumont, 2006). They can therefore be evaluated by solving an eigenvalue problem with modified boundary conditions, the open-circuit transducers condition giving the zeros; and the short-circuit condition for the poles of the open-loop transfer function. This is analogue to the well-known case of force-displacement SA pairs, where the poles and zeros of the open-loop transfer function correspond to the natural frequencies of the system with the degree of freedom of the SA pair, respectively, free or fixed. The difficulty with the nearly collocated configurations, traditionally used in active vibration control with piezoelectric patches, for the reasons cited above is that it is difficult to have a physical interpretation of the transmission zeros. In the coming sections, we aim to show that such a physical interpretation, although more complex, is possible and can lead to a better understanding of ways to improve the pole-zero



(a)



(b)

Fig. 2. A comparison of the FRFs corresponding to the ideally-located (self-sensing) and nearly-located piezoelectric SA patches attached to the cantilever plate at frequency ranges from: (a) 0 to 400 Hz, and (b) 2000 to 3000 Hz

distance, and hence the authority of active control systems based on nearly-located pairs of piezoelectric patches.

Unlike the self-sensing configuration, in the case of nearly-located configuration, both types of sensors (charge and/or voltage) can be used with voltage actuators. Therefore, it is also interesting to compare the two FRFs corresponding to: (i) the voltage actuator and voltage sensor, and (ii) the voltage actuator and charge sensor in the case of nearly-located configuration (Fig. 3).

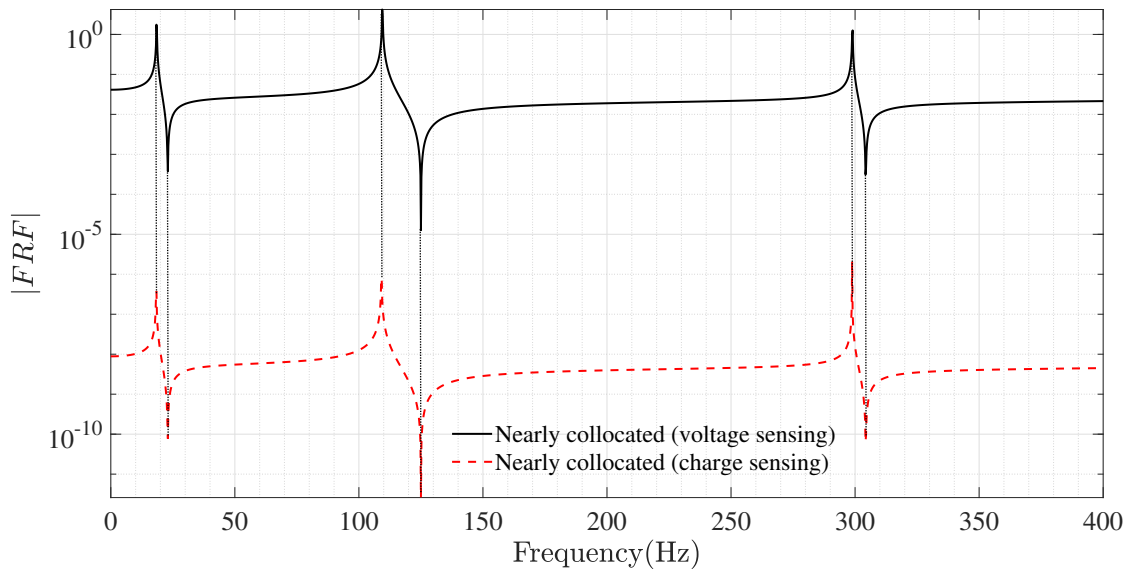


Fig. 3. A comparison of the FRFs corresponding to the nearly-located voltage-actuator/voltage-sensor and voltage-actuator/charge-sensor piezoelectric patches attached to the cantilever plate

It is noted that in both cases the poles and zeros are practically the same. However, the voltage sensing (or open-circuit) slightly stiffens the piezoelectric material due to the piezoelectric coupling due to which the eigenfrequencies are marginally higher (not more than 1%) in the case of voltage sensing (Balmes & Deraemaeker, 2013). Therefore, the current study though developed based on the voltage sensing also remains applicable to the charge sensing.

2.2 Model reduction and static correction

For practical applications, the complex structures are usually represented by large finite element models with thousands of DOFs. However, due to the interest in limited bandwidth and to

reduce the cost of computation, such finite element models may be reduced to the lower order by using an appropriate model reduction approach (Craig & Bampton, 1968; Wilson et al., 1982; Grimme, 1997; Besselink et al., 2013). In the present study, the modal truncation augmentation method is used which accounts for the model truncation error by adding a frequency independent feedthrough static correction term in the truncated model. For example, Eq. 7 can be rewritten as:

$$G_{as}(\omega) = \sum_{i=1}^M \frac{b_s \phi_i \phi_i^T b_a}{\mu_i (\omega_i^2 - \omega^2)} + R(\omega) \quad (8)$$

where $M < N_m + N_s$ and $R(\omega)$ is the frequency dependent residual term that can be expanded as follows:

$$R(\omega) = \sum_{i=M+1}^{N_m+N_s} \frac{b_s \phi_i \phi_i^T b_a}{\mu_i (\omega_i^2 - \omega^2)} \quad (9)$$

Consider that the bandwidth of excitation $[0, \omega]$ is such that $\omega \ll \omega_M$, where ω_M is the frequency of the M^{th} mode. Then, it can be assumed that the higher modes (greater than M) contribute statically to the overall response in the bandwidth of interest. This leads to the following approximation of $G_{as}(\omega)$:

$$G_{as}(\omega) \approx \sum_{i=1}^M \frac{b_s \phi_i \phi_i^T b_a}{\mu_i (\omega_i^2 - \omega^2)} + \sum_{i=M+1}^{N_m+N_s} \frac{b_s \phi_i \phi_i^T b_a}{\mu_i \omega_i^2} \quad (10)$$

The first term on the right hand side (R.H.S.) in Eq. 10 represents the dynamic response ($D_M(\omega)$) of the first M modes. The second feedthrough term, which is independent of frequency, is referred to as quasi-static correction (S_M) and accounts for the truncation of modes higher than M . The term S_M can be further written as:

$$S_M = \sum_{i=1}^{N_m+N_s} \frac{b_s \phi_i \phi_i^T b_a}{\mu_i \omega_i^2} - \sum_{i=1}^M \frac{b_s \phi_i \phi_i^T b_a}{\mu_i \omega_i^2} \quad (11)$$

where, the first term on the R.H.S. in Eq. 11 is the static response of the system ($G_{as}(0)$) and the second one is the total static response of the first M modes ($D_M(0)$). Thus, $S_M = G_{as}(0) - D_M(0)$ and the solutions of $D_M(\omega) + G_{as}(0) - D_M(0) = 0$ provide the transmission zeros. Thus, the accuracy of the transmission zeros would depend upon the: (i) number of modes included in the analysis (M), (ii) accuracy of the contribution of these modes ($D_M(\omega) - D_M(0)$)

which in turn depends on the accuracy of the first M mode shapes and eigenfrequencies (or poles), and (iii) accuracy of the static response which depends on the mesh accuracy of the finite element model. Therefore, for an accurate determination of the transmission zeros, the mesh size should be chosen such that the poles as well as the static response converge.

3 Finite Element Modelling and Analysis

As discussed above, piezoelectric structures require finite element modelling to determine the transmission zeros. This section provides a general overview of the development and analysis of the finite element models used in the current study.

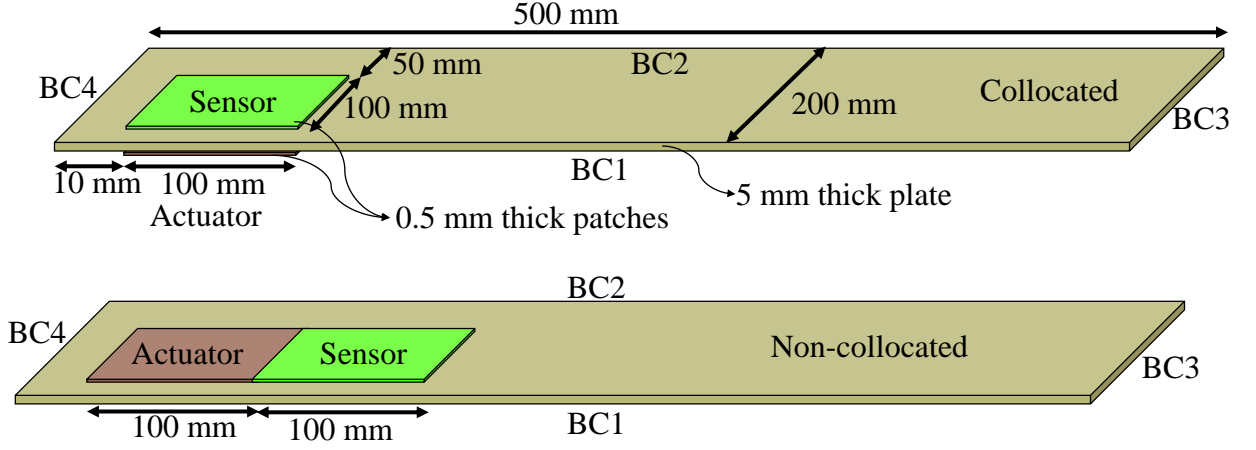
3.1 Geometrical configuration

This study investigates various cases of a thin rectangular aluminium plate equipped with a single pair of piezoelectric voltage sensor and voltage actuator patches. Three types of boundary conditions (cantilever, clamped-clamped, and all-clamped) and two types of arrangement of piezoelectric SA patches (nearly-collocated, referred as ‘collocated’ and non-collocated) are considered as shown in Fig. 4. The different combinations of the boundary conditions and the patch-arrangement are referred by a case-number as shown in Fig. 4.

3.2 Material properties

Aluminium is used as the plate material with Young’s modulus of 72 GPa, Poisson’s ratio of 0.3, density of 2769.2 kg/m³, and the damping is assumed to be negligible (0.001%). The transversely isotropic Z-polarized Lead-Zirconate-Titanate (PZT) is used as piezoelectric material for sensor and actuator patches with (i) piezoelectric coefficients ($[d]$):

$$\begin{bmatrix} 0 & 0 & 0 & 0 & d_{15} & 0 \\ 0 & 0 & 0 & d_{24} & 0 & 0 \\ d_{31} & d_{32} & d_{33} & 0 & 0 & 0 \end{bmatrix} = \begin{bmatrix} 0 & 0 & 0 & 0 & 5.5 & 0 \\ 0 & 0 & 0 & 5.5 & 0 & 0 \\ -1.8 & -1.8 & 4 & 0 & 0 & 0 \end{bmatrix} \times 10^{-10} \text{m/V}$$



BC1	BC2	BC3	BC4	Name	Collocated	Non-collocated
	Free		Clamped	Cantilever plate	Case-1C	Case-1NC
	Free		Clamped	Clamped-clamped plate	Case-2C	Case-2NC
			Clamped	All-clamped plate	Case-3C	Case-3NC

Fig. 4. A pictorial representation of different configurations of the thin rectangular plate equipped with piezoelectric patches

(ii) permittivity ($[\epsilon^T]$):

$$\begin{bmatrix} \epsilon_{11}^T & 0 & 0 \\ 0 & \epsilon_{22}^T & 0 \\ 0 & 0 & \epsilon_{33}^T \end{bmatrix} = \begin{bmatrix} 1650 & 0 & 0 \\ 0 & 1650 & 0 \\ 0 & 0 & 1750 \end{bmatrix} \epsilon_0$$

and (iii) mechanical properties: (a) Young's modulus: $E_1 = E_2 = 62.11$ GPa (perpendicular to poling direction) and $E_3 = 48.31$ GPa (along the poling direction), (b) density: 7800 kg/m³, and (c) Poisson's ratio: $\nu_{12} = \nu_{21} = 0.3242$, $\nu_{31} = \nu_{32} = 0.30$, and $\nu_{13} = \nu_{23} = 0.39$, where, $\epsilon_0 = 8.854 \times 10^{-12}$ F/m is the permittivity of vacuum. The subscripts 1 and 2 refer to the X and Y directions in the plane of the piezoelectric patch (transversely isotropic) while the subscript 3 refers to the poling direction of the patches (i.e., along their thickness). It is also important to mention that the electrodes are considered to be uniformly distributed on the piezoelectric sensor and actuator patches.

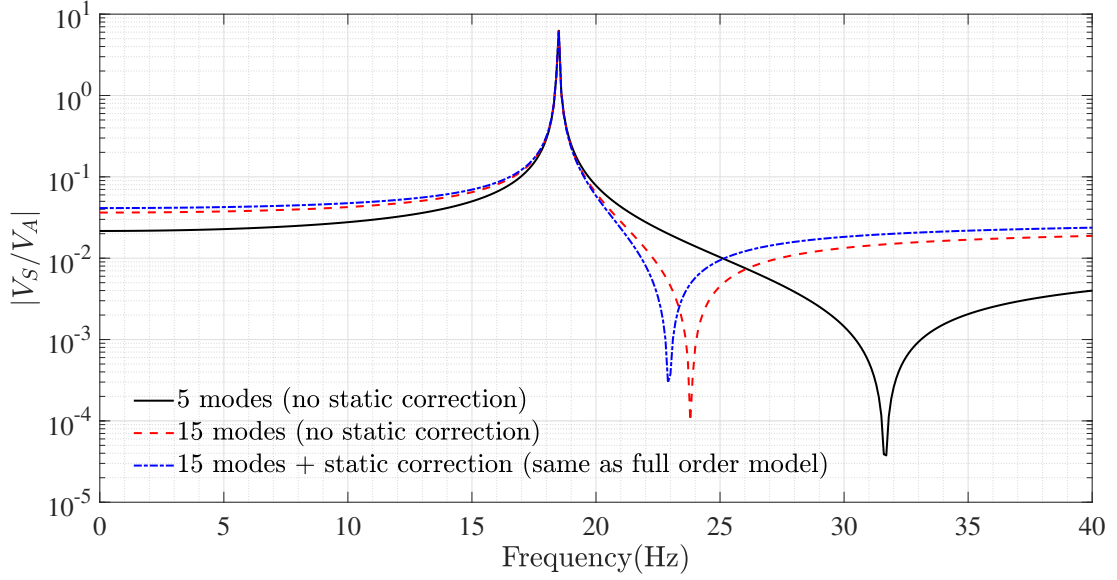
3.3 Element properties

Since the structures are equipped with rectangular piezoelectric patches, four noded linear shell elements are used. Furthermore, to account for the effects of rotary inertia and shear deformations, the Mindlin shell elements with a shear correction factor of $5/6$ (Rao, 2007) are used in the model.

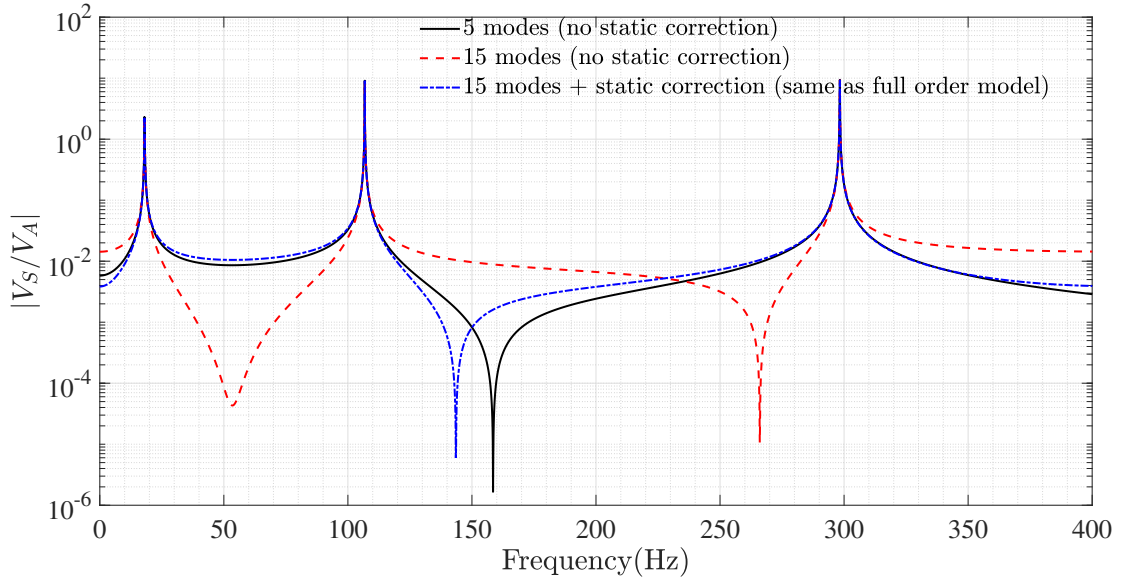
Using the above data, finite element models are developed and their dynamics (poles, zeros, static response, static correction, mode shapes, and FRF) are evaluated using Structural Dynamics ToolBox (SDT) of MATLAB (Balmes & Deraemaeker, 2013).

4 Effects of Model Truncation

It is analytically explained in the Section 2.2 that the accuracy of the transmission zeros hinges on the number of the first M modes included in the analysis and the correction for the excluded modes. This section quantitatively demonstrates the effect of model truncation through the examples of aluminium cantilever plate equipped with (i) collocated (Case-1C) and (ii) non-collocated (Case-1NC) piezoelectric SA patches (Fig. 4). To explicitly highlight the effect of model truncation, mesh size is taken as 1 mm because, as it will be seen later, 1 mm mesh size is fine enough to avoid any mesh convergence related errors. The evolution of the FRF between voltage sensor and voltage actuator is studied including first $M = 5$ and 15 modes without static correction and the full order model as shown in Fig. 5. For the convenience of demonstration, the analysis is kept limited to the first transmission zero only. The full order model can be solved using the in-built solver 'fe_simul' in SDT. However, this approach is computationally costly. Therefore, in the present example, the FRF corresponding to the 15 modes with static correction is considered equivalent to the full order model, specially in the frequency range considered in the example. To ensure the convergence, the FRF corresponding to the 15 modes with static correction is compared with the FRF corresponding to the 50 modes with static correction and a perfect overlap is observed between the two FRFs.



(a)



(b)

Fig. 5. The influence of model truncation on the FRF corresponding to the: (a) collocated (Case-1C) and (b) non-collocated (Case-1NC) piezoelectric SA patches attached to the cantilever plate

Although in the case of collocated patches, the FRF gradually shifts towards the converged values when increasing the number of considered modes, the actual convergence is achieved only after including the static correction (Fig. 5 a). Moreover, the errors due to model truncation become much more pronounced in the case of non-collocated patches (Fig. 5 b). Also, the FRF of the non-collocated case does not seem to follow monotonic trend while shifting towards the converged FRF.

It is also interesting to compare these results with the case when the cantilever plate is equipped with the collocated force-displacement SA pair as shown in Fig. 6. It can be seen very clearly that, unlike the case of piezoelectric SA patches, the FRF converges rapidly with increasing number of modes in the case of force-displacement SA pair.

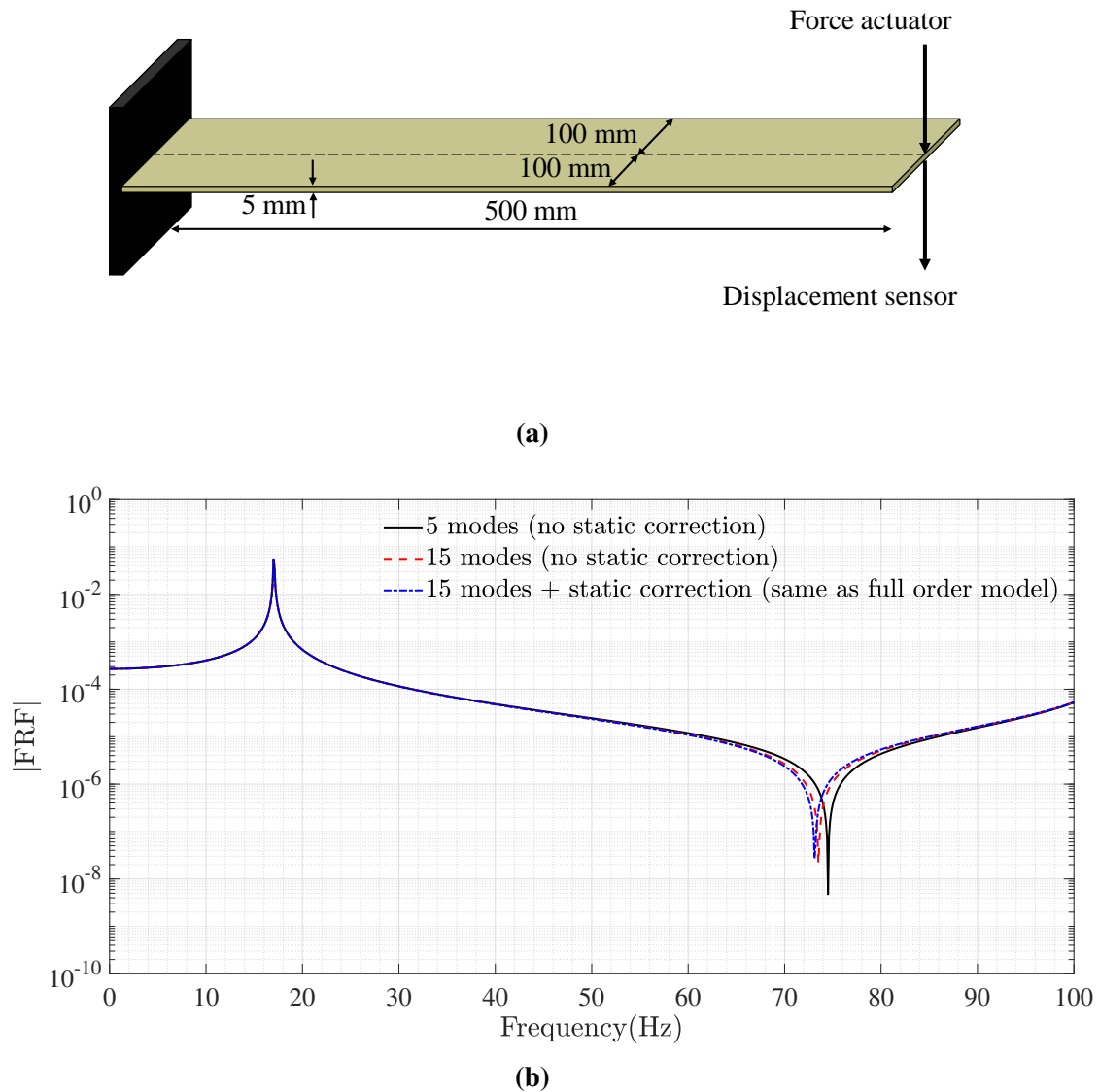
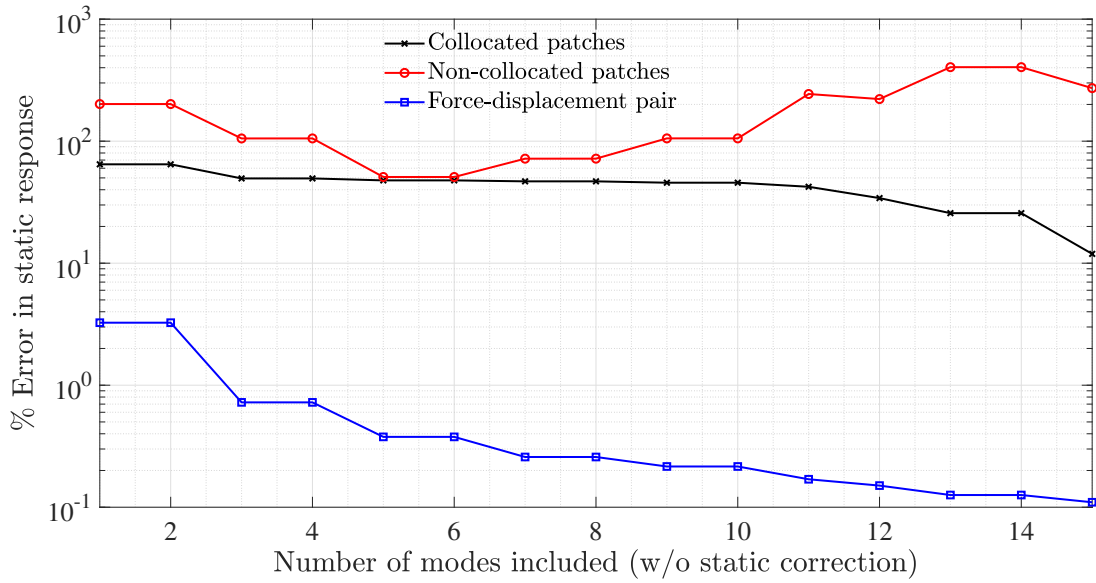
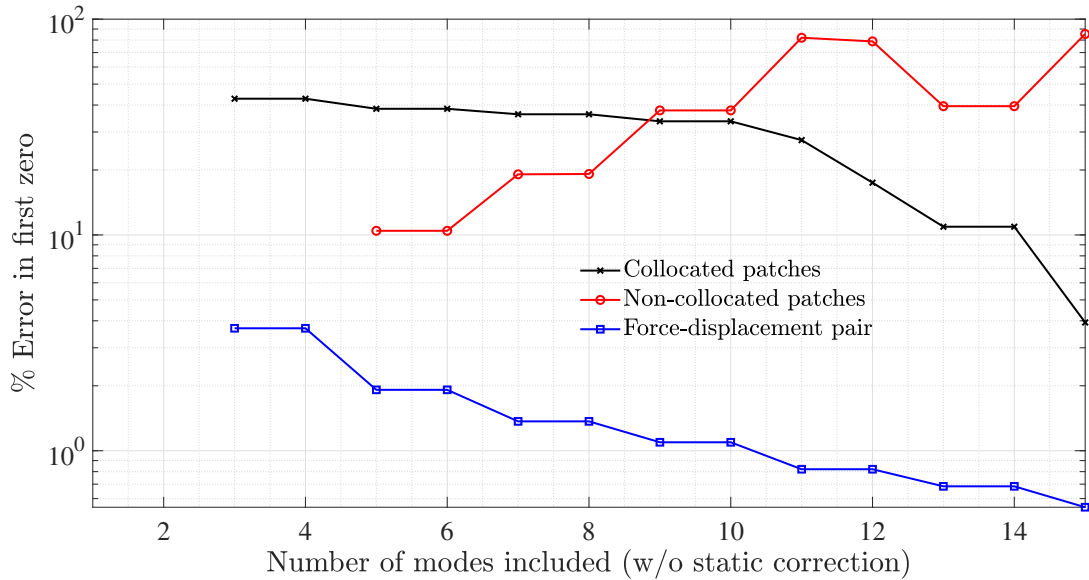


Fig. 6. (a) The cantilever plate equipped with force (actuator)-displacement (sensor) pair and (b) the influence of model truncation on the FRF between force-displacement SA pair attached to the cantilever plate

A comparative study of the errors in the static response and the first transmission zero, for the three cases (Case-1C, Case-1NC, and collocated force-displacement SA pair), is also carried out as shown in Fig. 7. The percentage errors are computed with respect to the corresponding converged FRFs.



(a)



(b)

Fig. 7. A comparison of the impact of model truncation on: (a) static response, and (b) first transmission zero, corresponding to the collocated and non-collocated piezoelectric SA patches and force-displacement SA pair attached to the cantilever plate

As already observed in the respective FRFs (Figs. 5 and 6b), the errors are smallest in the case of force-displacement pair and largest in the case of non-collocated patches (Fig. 7). Interestingly, in the case of non-collocated patches, there is no gradual reduction of errors with increasing number of modes. It is also worth mentioning here that Williams (1992b) noted the similar non-monotonic error reduction in the case of transmission zeros of the non-collocated

force-displacement SA pair. However, in the other two cases, the errors decrease monotonically with more number of modes included in the analysis. It is also evident that in the case of force-displacement SA pair, the errors become insignificant ($<1\%$) even without including the static correction, whereas, the errors are large ($\approx 10\%$) in the case of piezoelectric patches. This clearly demonstrates that the static correction becomes significantly important in the case of piezoelectric structures. This phenomenon can be explained intuitively by comparing the static deformed shapes (static response) of the piezoelectric plate and the plate with force-displacement pair as shown in Fig. 8.

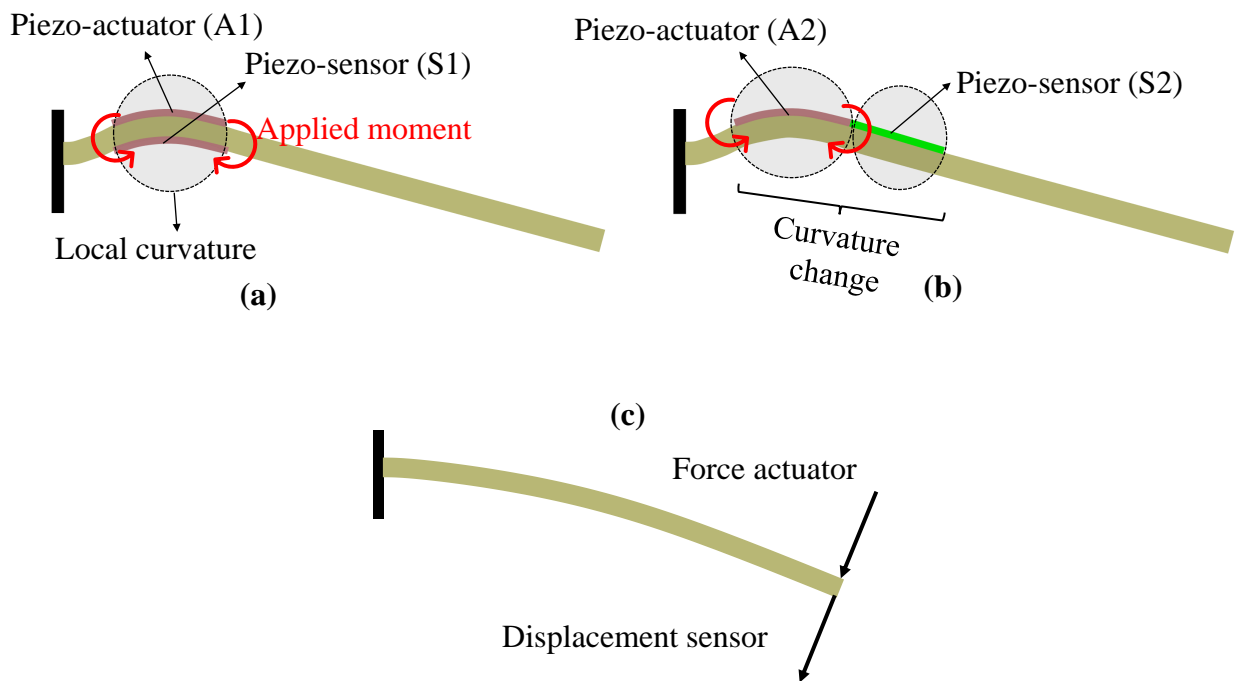


Fig. 8. The representative static deflected shapes of the cantilever plate equipped with (a) collocated (Case-1C) and (b) non-collocated (Case-1NC) piezoelectric SA patches, and (c) force-displacement SA pair

The sensing-actuation mechanism of piezoelectric patches is governed by the strain at the location of their placement on the host-structure. It is also well known, from the classical thin plate theory, that the strains are directly proportional to the deformation curvature (Timoshenko & Woinowsky-Krieger, 1959). Thus, the sensing-actuation mechanism of the piezoelectric patches is linked with the curvature of the deformed shape unlike the force-displacement SA pair which depends only on the magnitude of the deformation. As can be seen in Figs. 8(a) and (b), there is a localized curvature due to the applied moments by the actuator patches

(A1 and A2). Although the curvatures are the same for the actuators A1 and A2, the sensors S1 (collocated case) and S2 (non-collocated case) are subjected to different curvatures. For an accurate determination of the static response (and the transmission zeros), it is necessary to precisely capture this local curvature. The geometrical curvature can be represented as a 2^{nd} order derivative of the deformation function which can be further written as a linear combination of the different mode shapes. However, the mode shapes (which can be assumed to be independent of SA patches for small piezoelectric patches), usually, do not include any information on the local deformation, therefore, it is unlikely that the local deformation can be accurately represented by a linear combination of finite number of mode shapes without including a static correction. In the case of collocated patches (A1 and S1), only single local curvature needs to be represented accurately, whereas, in the non-collocated case (A2 and S2), two different curvatures are required as shown in Fig. 8 (b). Thus, the accuracy in the non-collocated case depends on the coupled accuracy of the two different curvatures. It is quite possible that a particular mode shape can tentatively represent one of the local curvatures but at the same time the same mode shape may misrepresent the second local curvature which seems to be a possible reason behind the non-monotonic error reduction in the non-collocated case. Therefore, the non-collocation further complicates the problem and the static correction becomes even more important in this case. On the contrary, there is no localized curvature in the static deformed shape of the force-displacement pair (Fig. 8c) and the static deformed shape can be accurately represented as a linear combination of a few mode shapes. Thus, the above discussion clearly describes the reason behind the higher errors caused by the model truncation in the case of piezoelectric patches compared to the force-displacement SA pair.

5 Effects of Model Discretization

The previous section discussed the effect of model truncation on the accuracy of the predicted poles and zeros, and the current section discusses the effect of mesh size on the same quantities. While the effect of mesh size on the poles has been largely studied in the literature, it is not the case for zeros. The aim of this section is therefore to show that meshing rules are different to

accurately predict the poles than for zeros. For instance, consider the cantilever plate equipped with collocated piezoelectric SA patches (Case-1C) as shown in Fig. 4. To study the effects of mesh discretization, the percentage error E_{Δ} (corresponding to a mesh size Δ) is computed as:

$$E_{\Delta} = \frac{|P_{\Delta} - P_{\Delta_c}| \times 100}{P_{\Delta_c}} \quad (12)$$

where, P_{Δ} and P_{Δ_c} are the values of the parameter of interest corresponding to the mesh size Δ and Δ_c , respectively, such that the mesh corresponding to the size Δ_c is fine enough to lead to the converged value of the parameter. In the present case, Δ_c is taken as 1 mm (the justification is discussed a bit later) and the corresponding FRF between the piezoelectric voltage actuator (V_A) and voltage sensor (V_S) is shown in Fig. 9.

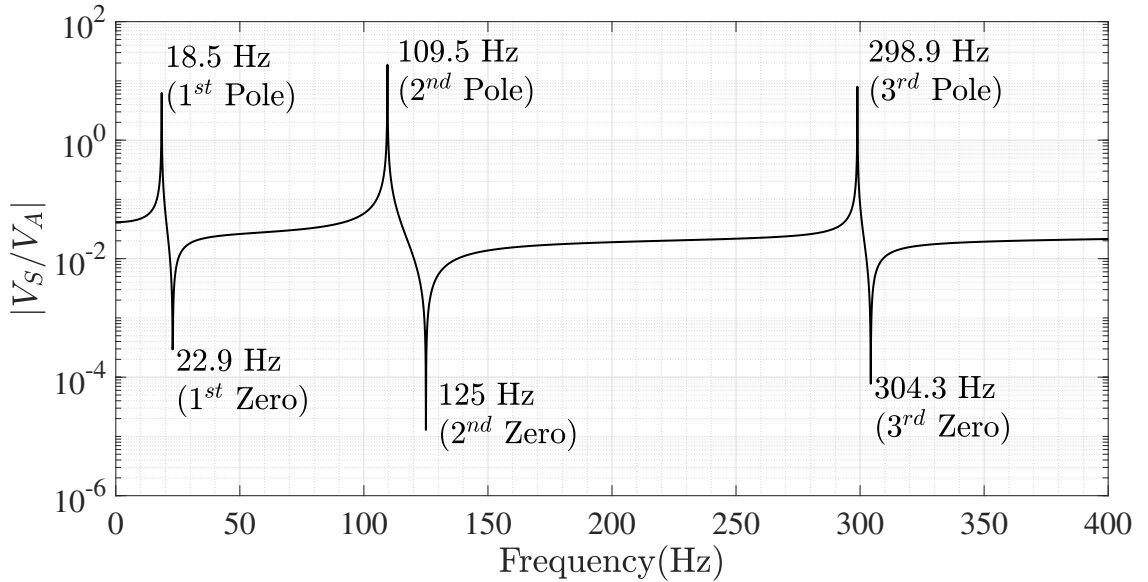


Fig. 9. The FRF between collocated piezoelectric (voltage) sensor/ (voltage) actuator patches attached to the cantilever plate for a mesh size of 1 mm

To ensure that there are no effects of model truncation, the analysis is carried out by retaining the first 50 modes with static correction which is equivalent to the full order model in the frequency range considered here. The first three poles appear at 18.5 Hz (1st Pole), 109.5 Hz (2nd Pole), and 298.9 Hz (3rd Pole) and the first three zeros appear at 22.9 Hz (1st Zero), 125 Hz (2nd Zero), and 304.3 Hz (3rd Zero) in the FRF. It is also worth mentioning that the frequencies 91.2 Hz (first torsion mode) and 288.2 Hz (second torsion mode) correspond to the

pole-zero cancellation and, therefore, do not appear in the FRF because torsion modes are not excited by the piezoelectric actuator in the present case. The variation of errors (with reducing mesh size) in the first three poles and zeros and in the static response are shown in Fig. 10, which clearly justifies that Δ_c can be safely taken as 1 mm because the errors for 5 mm mesh (w.r.t. to 1 mm mesh) are insignificant (less than 0.1%).

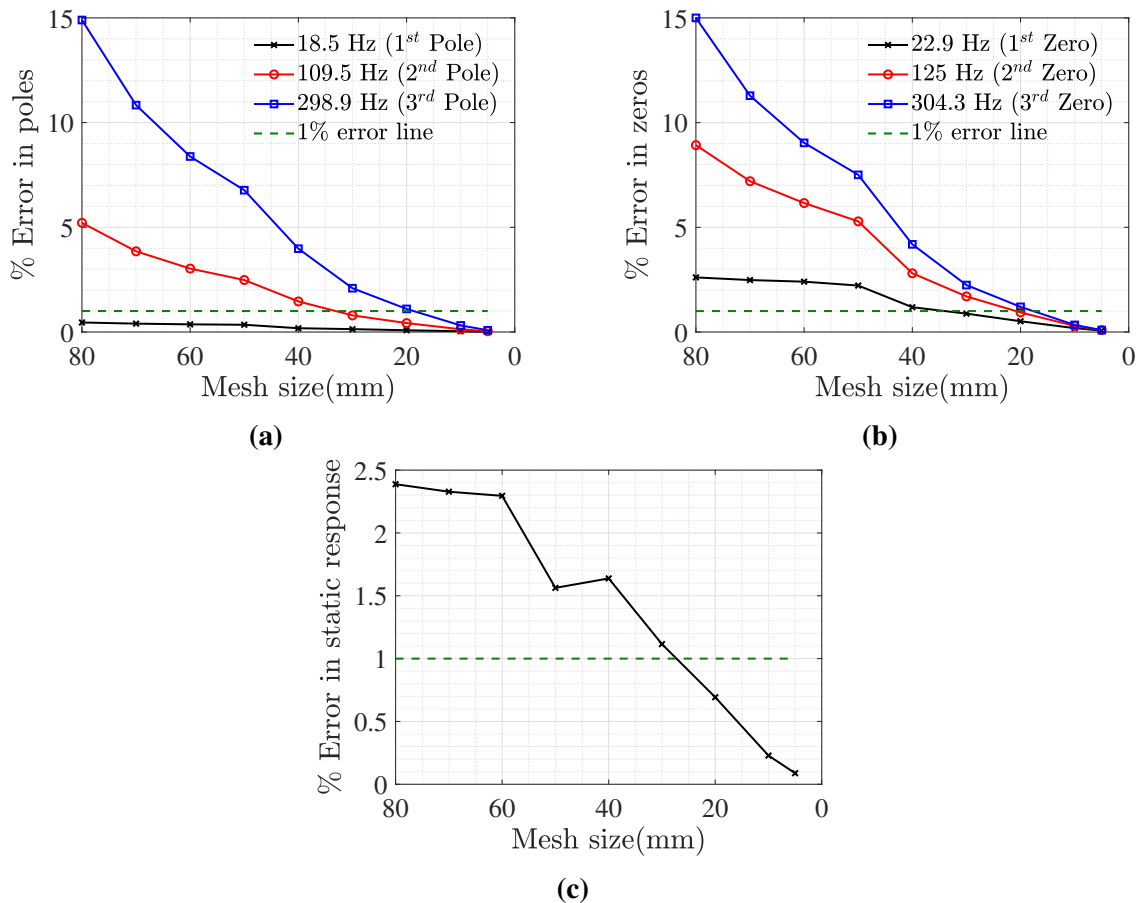


Fig. 10. Effect of the mesh discretization on: (a) first three poles, (b) first three zeros, and (c) static response of the FRF between collocated piezoelectric SA patches attached to the cantilever plate

It can be observed that the higher order modes need more refined mesh compared to a lower order mode for achieving similar level of accuracy. For example, second and third poles require a mesh size of less than 35 mm and 20 mm, respectively, to achieve an error of less than 1%, whereas the errors in the first pole are not significant even for a very coarse mesh. This can be explained by comparing the first three bending mode shapes of the plate as shown in Fig. 11.

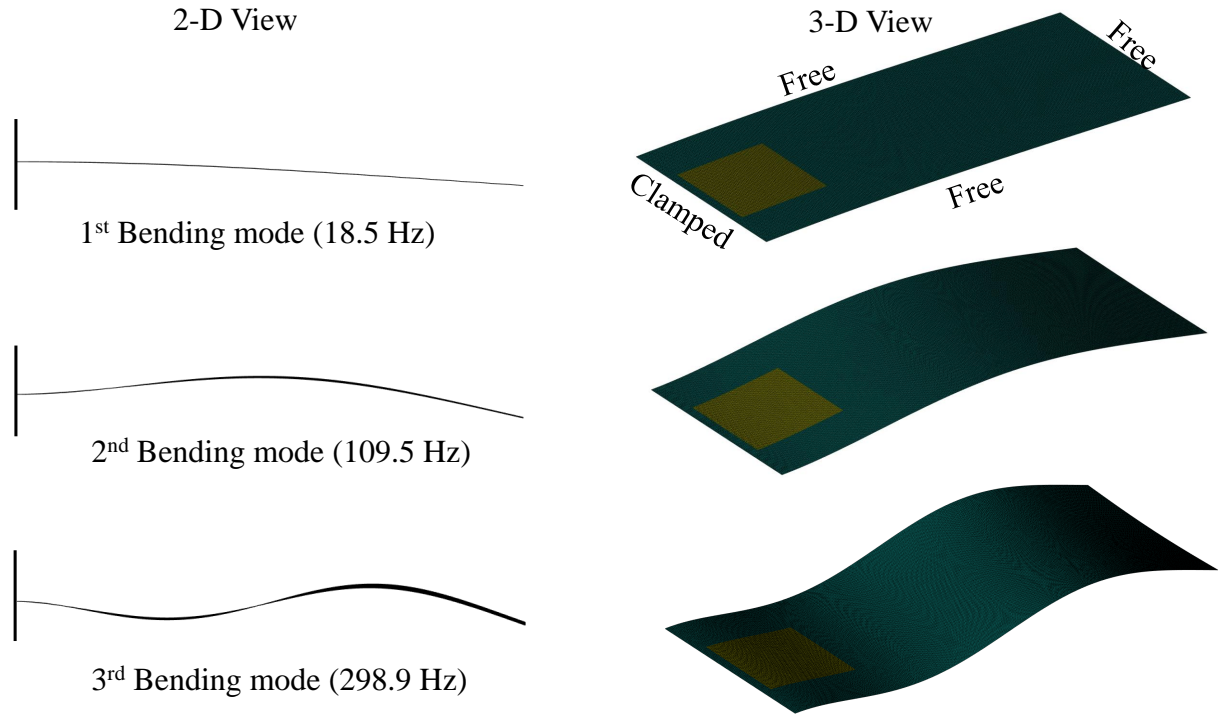


Fig. 11. The mode shapes of the first three bending modes of the cantilever plate equipped with collocated piezoelectric patches (Case-1C)

Using the analytical expressions of bending mode shapes of a cantilever beam (Rao, 2007), the bending wavelength (λ_n) of a cantilever beam (of length L) in the n^{th} bending mode can be approximated as: $\lambda_n = 4L/(2n - 1)$. For a mesh size of Δ , there would be λ_n/Δ number of elements per wavelength. It can be observed from Fig. 12 that, in the present example, at least 22 and 70 elements per wavelength are required to achieve an accuracy (on poles) of 1% and 0.1%, respectively. It is also interesting to note that the generally considered rule-of-thumb of 10 elements per wavelength leads to an error of around 4% in the current example (Fig. 12). Therefore, for a fixed mesh size, the number of elements per wavelength reduces with increasing mode order which leads to the higher errors for higher order modes.

Figure 10 illustrates as well that the mesh convergence also depends upon the parameter of interest. In particular, the convergence of the transmission zeros is slower compared to the poles because the zeros depend on: (i) the dynamic response of modes included in the analysis and (ii) static response contribution of the truncated modes. Thus, their convergence would also depend upon the convergence of the poles as well as the static response. This also implies that convergence of poles does not guarantee the convergence of zeros due to which it is always

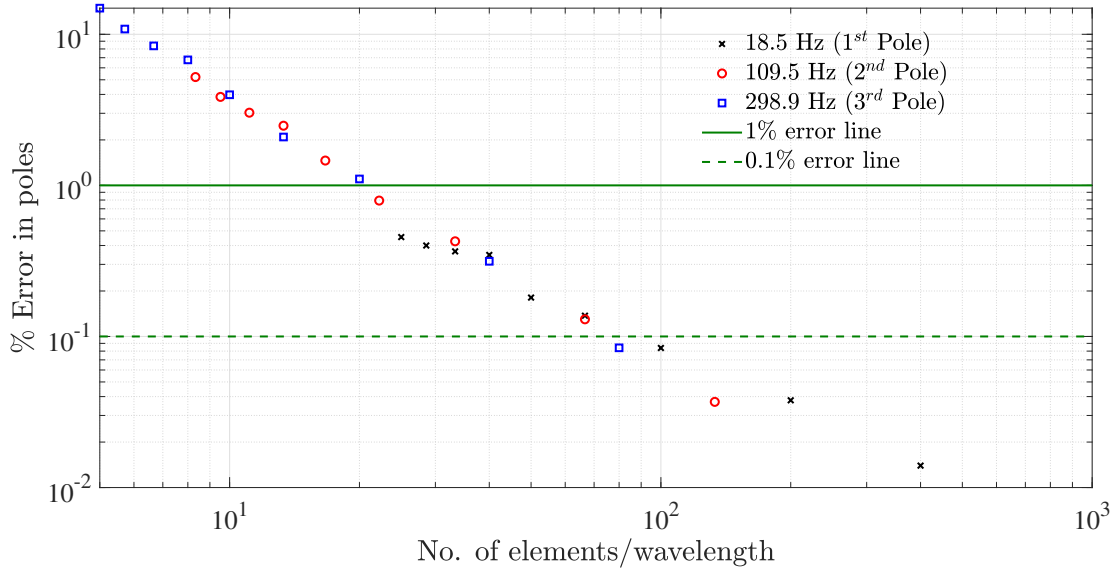


Fig. 12. The variation of errors in the estimation of poles with increasing number of elements per (bending) wavelength in the case of cantilever plate (Case-1C)

necessary to ensure the convergence of zeros. For example, to achieve an accuracy of less than 1% on second order zero, one needs to use a mesh size smaller than 20 mm, i.e., finer than the one required for the second order pole (Fig. 10).

Here it would also be worth comparing the mesh convergence results of collocated piezoelectric SA patches with the case of collocated force-displacement pair of Fig. 6 (a). A comparison of mesh convergence of the static response and the first transmission zero for the two cases is shown in Fig. 13.

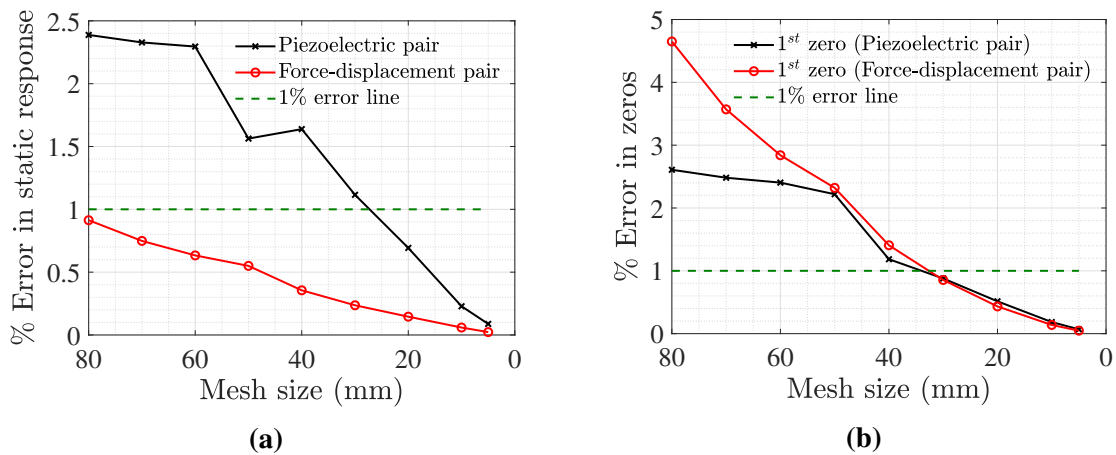


Fig. 13. The influence of mesh discretization on: (a) static response and (b) first transmission zero in the case of force-displacement SA pair and collocated piezoelectric SA patches attached to the cantilever plate (case-1C)

The slower convergence of static response in the case of piezoelectric patches can be easily explained by observing the static deformed shapes for the two cases as shown in Figs. 8 (a) and (c). As discussed previously, accuracy of the static response relies on the correct representation of the static deformed shape. Due to the presence of a local curvature, a more refined mesh is required in the case of piezoelectric patches for achieving the accuracy similar to the force-displacement pair. However, it is interesting to note that the convergence of the first transmission zero is marginally slower in the case of force-displacement pair compared to the piezoelectric patches for coarser meshes. This counter-intuitive phenomenon seems logical due to the following two contrasting factors contributing to the convergence of the zero: (i) slower convergence of static response for piezoelectric patches (Fig. 13 a) and (ii) smaller wavelength of the deflected shape, at first zero frequency (73.2 Hz), of the force-displacement case (Fig. 14). Thus, this example clearly shows that the mesh convergence is jointly controlled by the local curvature and the bending wavelength.

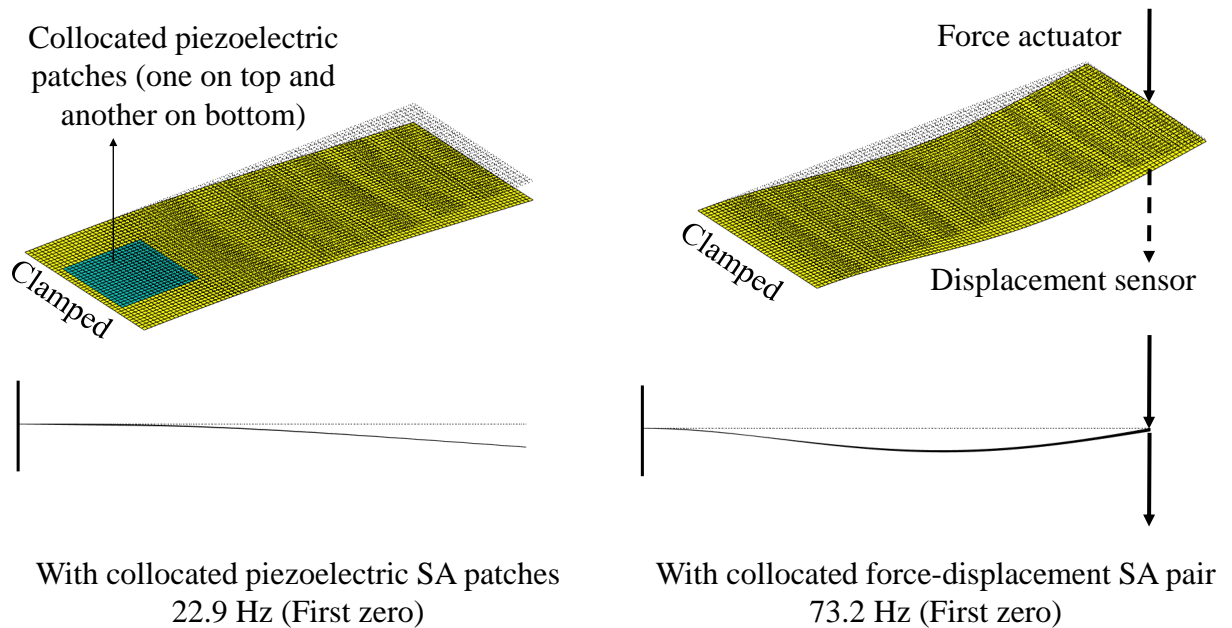


Fig. 14. The deflected shapes of the cantilever plate at first transmission zero frequency in the case of collocated piezoelectric SA patches and force-displacement SA pair

5.1 Effect of boundary conditions

The boundary conditions significantly affect the wavelength of the mode shapes and the static response and, thus, also affect the mesh convergence rate. To illustrate the effect of boundary conditions, the three cases with collocated piezoelectric patches attached to the: (i) cantilever plate (Case-1C), (ii) clamped-clamped plate (Case-2C), and (iii) all-clamped plate (Case-3C) are considered (Fig. 4). With increasing boundary constraints (Fig. 15): (i) the bending wavelength of the first mode reduces, leading to a reduction of the number of elements per wavelength for a given mesh size, (ii) additional local curvature appears in the static deformed shape due to the localized piezoelectric actuation, and (iii) in the case of all-clamped plate, a double curvature is observed.

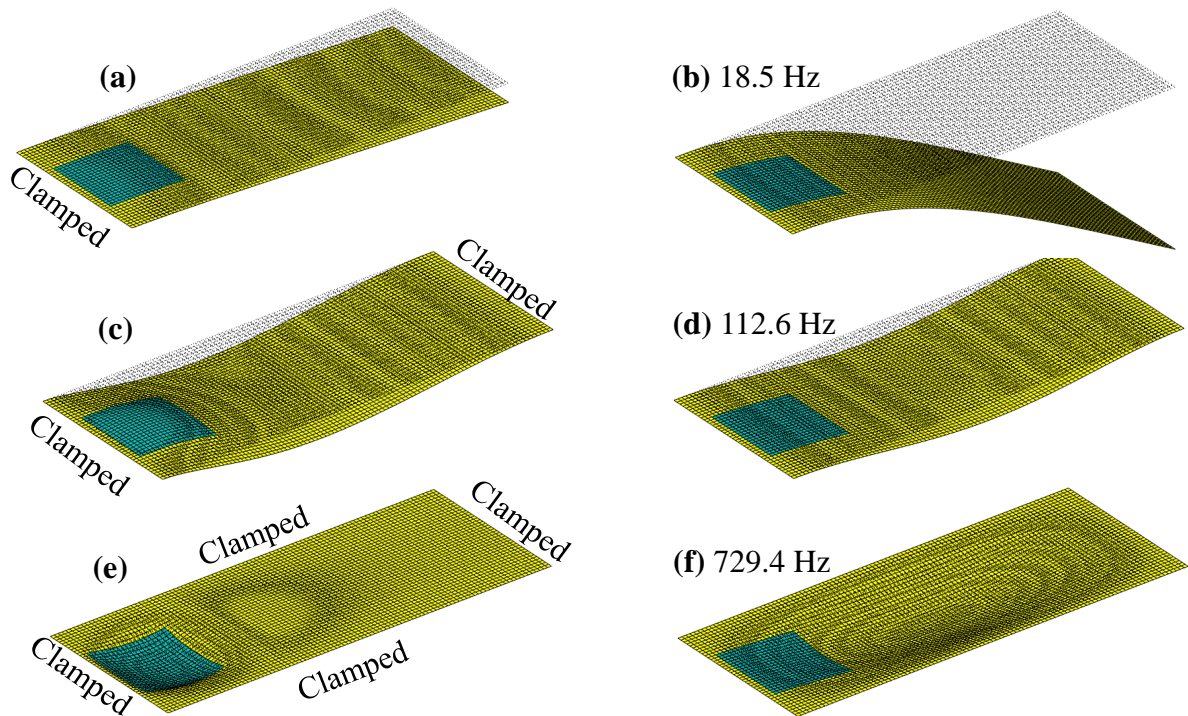


Fig. 15. The deflected shapes of static response and first mode, respectively, of (a,b) cantilever (Case-1C), (c,d) clamped-clamped (Case-2C), and (e,f) all-clamped plate (Case-3C) equipped with collocated piezoelectric SA patches

Therefore, a finer mesh is required for the convergence of the poles and the static response, and, consequently, for the transmission zeros when the boundary constraints are increased, as demonstrated in Fig. 16. For example, to achieve an accuracy of 1% on the all the three parameters (1^{st} pole, 1^{st} zero, and static response), a mesh size of less than 27 mm, 15 mm, and

13 mm is required, respectively, for the cantilever, clamped-clamped, and all-clamped plate.

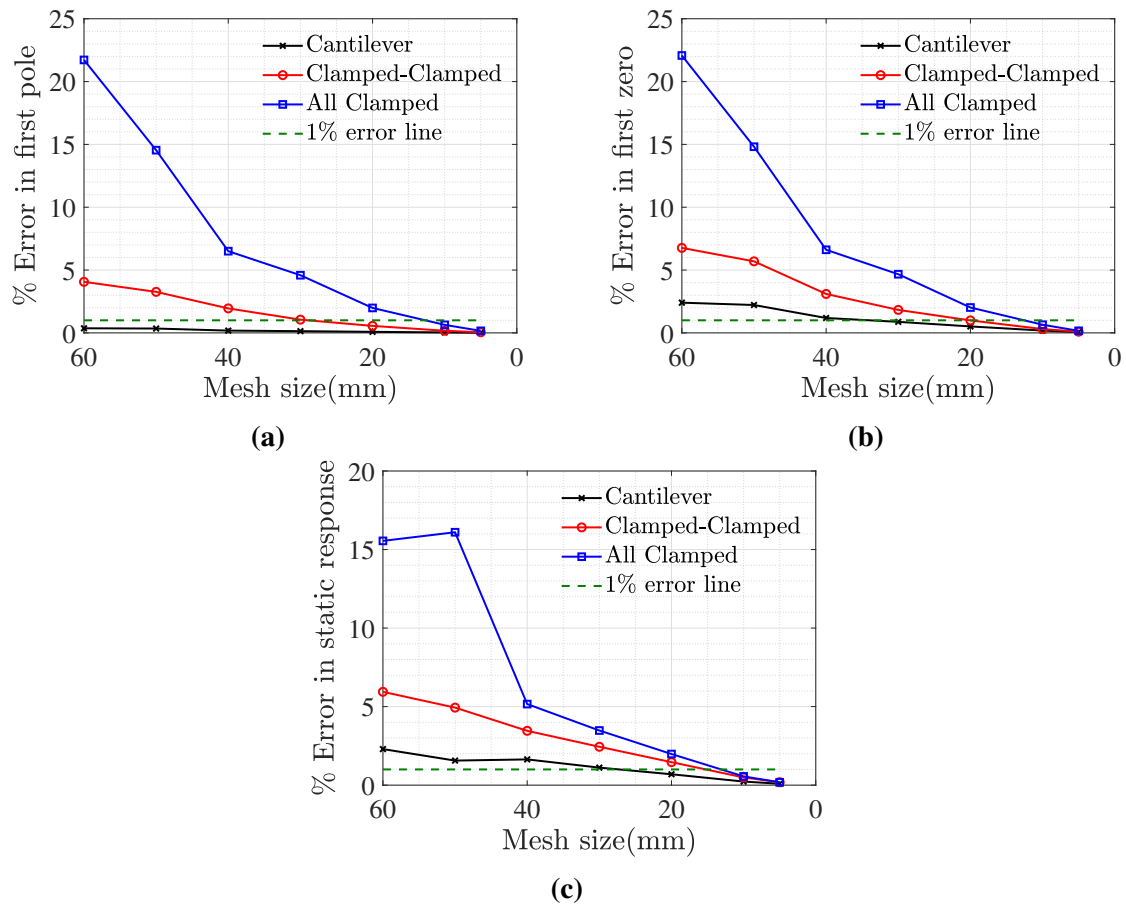


Fig. 16. Effect of boundary condition on the mesh convergence of: (a) first pole, (b) first zero, and (c) static response of the FRF between collocated piezoelectric SA patches attached to the plate

5.2 Effect of non-collocation

In some of the practical applications (e.g. [Hariri et al., 2015](#)), the piezoelectric patches may be required to be arranged in a non-collocated configuration. In view of this, it is also important to investigate the effect of non-collocation on mesh convergence rate. In the present study, non-collocation is considered as presented in Fig. 4. The FRF corresponding to the non-collocated case (Case-1NC) is compared with the collocated one (Case-1C) as shown in Fig. 17. The poles of the collocated case almost overlap with the poles of the non-collocated configuration with minor differences due to the local mass and stiffness added by the piezoelectric patches. As expected there is a significant difference in the static response and, subsequently, between the transmission zeros of the two cases. Also, the pole-zero interlacing pattern disappears in

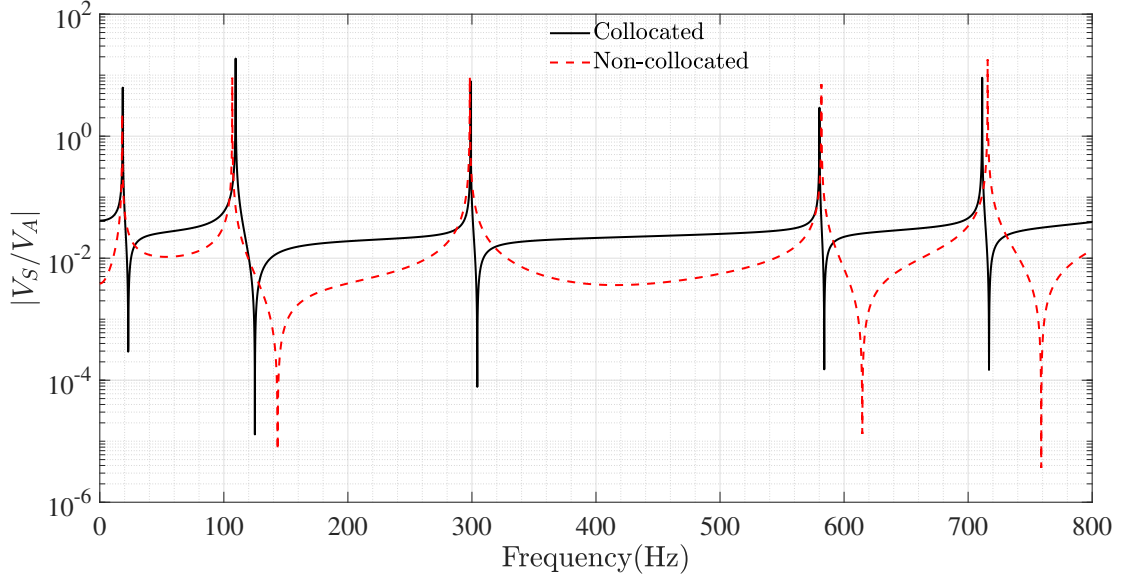


Fig. 17. A comparison between the FRFs (with 1 mm mesh size) corresponding to the collocated (Case-1C) and non-collocated (Case-1NC) piezoelectric SA patches attached to the cantilever plate

the non-collocated case. The difference in the static response can be described qualitatively by comparing the static deflected shapes of the two cases as shown in Figs. 8 (a) and (b). Because the deformation curvatures are linked to the strain distribution and the sensing-actuation mechanism of piezoelectric patches depends on the strain, the curvature change at the sensor location relative to the actuator location governs the static response. Thus, in the non-collocated case, the curvature difference between the sensor and actuator locations needs to be captured accurately in order to precisely determine the static response. Nevertheless, in the collocated case, there is no curvature difference between the sensor and actuator locations which explains why a finer mesh is required to achieve a similar accuracy in the static response for the non-collocated configuration (Fig. 18a). Clearly, the slower convergence of the static response causes the slower convergence of zeros in the non-collocated case (Fig. 18b). For example, a mesh size of 15 mm is small enough to obtain an accuracy of 1% on the first three zeros of the collocated case (case-1C), however, the mesh needs to be refined further to 10 mm for the same accuracy on the first zero of the non-collocated case (Case-1NC).

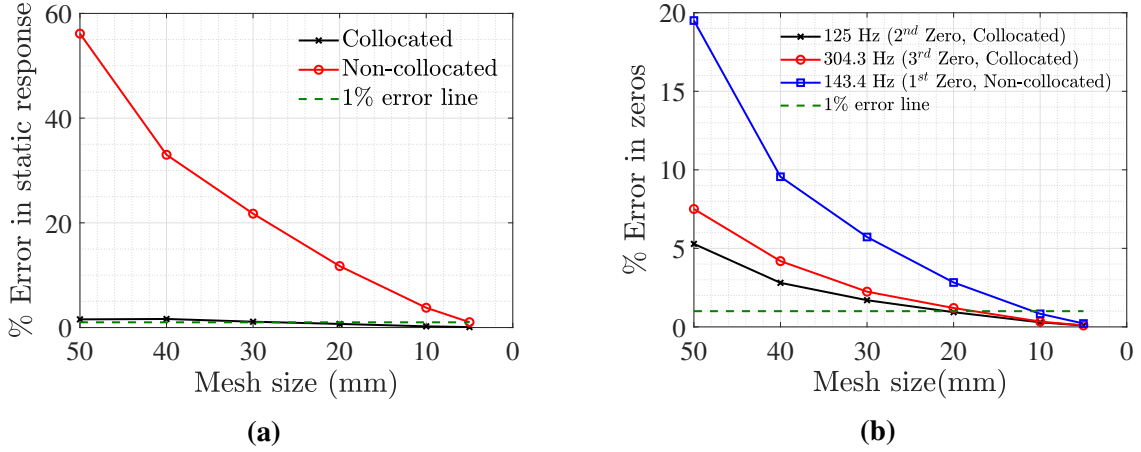
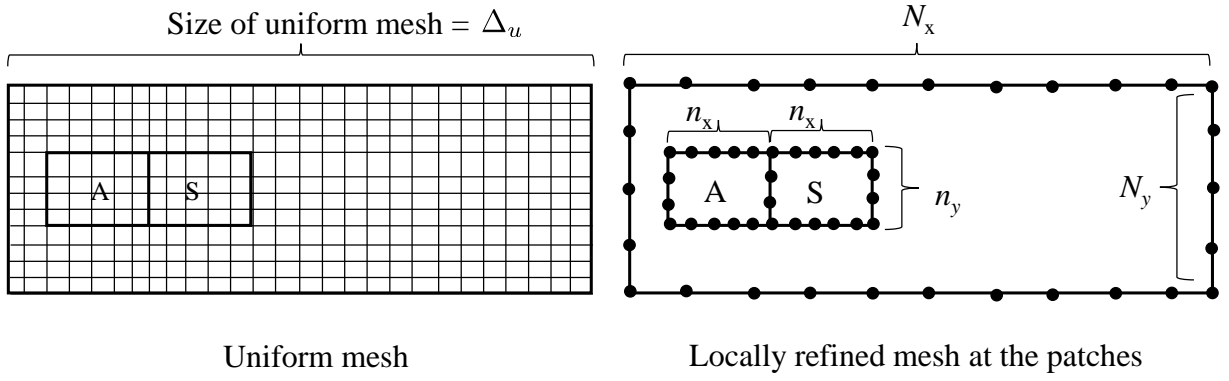


Fig. 18. A comparison between the mesh convergence for: (a) static response and (b) transmission zeros corresponding to the collocated (Case-1C) and non-collocated (Case-1NC) piezoelectric SA patches attached to the cantilever plate

5.3 Local mesh refinement

Since the poles are global characteristics and are represented by mode shapes of a system, it requires only global refinement of the mesh for the convergence of the poles. However, the static response (and, hence, the transmission zeros) are highly dependent on local deformation curvature at the location of the patches. Consequently, an additional mesh refinement may be needed for accuracy, which significantly adds to the cost of computation. For example, in the case of non-collocated piezoelectric patches attached to the cantilever plate (Case-1NC), the model with uniform mesh size of 1 mm (i.e., 101404 nodes \times 6 mechanical DOFs + 2 electrical DOFs) takes almost 262 seconds (on a 64-bit Windows-10 platform computer with an Intel(R) Core(TM) i5-8265U CPU at 1.80 GHz with 32GB RAM) to obtain the FRF. There is no doubt that for the complex structures (such as curved shells or rings), a very high mesh density may be required and the computation time would be much higher.

Since the piezoelectric actuators produce localized strains (or deformation curvature), it may be a numerically efficient option to have a high mesh density only at the location of the patches and a low mesh density at other regions of the structure. The global mesh size may be governed by the pole convergence and the local mesh size (near the patches) may be governed by the convergence of the static response. In view of this, a local mesh refinement strategy is illustrated on the current example of cantilever plate equipped with non-collocated piezoelectric



A = Piezoelectric actuator patch

S = Piezoelectric sensor patch

N_x = The number of nodes on the length of the plate

N_y = The number of nodes on the width of the plate

n_x = The number of nodes on the length of the piezo-patches

n_y = The number of nodes on the width of the piezo-patches

Fig. 19. A representative diagram for uniform mesh and locally refined mesh

patches (Case-1NC) as shown in Fig. 19. In view of the previous discussions, it is clear that a mesh converging for a higher order pole would also ensure the convergence of the lower order poles. For example, to illustrate the methodology of deciding the global mesh size (Δ_g), the convergence of 5th order pole is studied as shown in Fig. 20(a). For the 500 mm long cantilever plate, the wavelength of the 5th bending mode is 222.2 mm. From Fig. 20(a), it is straightforward to notice that around 22 elements per wavelength are sufficient to ensure an error of less than 1%. This corresponds to a global mesh size of $\Delta_g = 222.2/22 \approx 10$ mm. Thus, the number of nodes on boundary of the cantilever plate along the length (N_x) and the number of nodes on boundary of the cantilever plate along the width (N_y) can be written as $L/\Delta_g + 1$ and $W/\Delta_g + 1$, respectively. In the present example, $N_x = 500/10 + 1 = 51$ and $N_y = 200/10 + 1 = 21$. Once the global mesh size has been converged upon, the local mesh size (Δ_l) is found by studying the convergence of static response as a function of Δ_l/Δ_g (Fig.20 b). For the local mesh refinement in this study, an open source finite element mesh generator (Gmsh (Geuzaine & Remacle, 2009)) is utilized. The local mesh convergence indicates that a local refinement of 80% (i.e, $\Delta_l = 0.2 \times \Delta_g = 2$ mm is sufficient for the convergence of the static response and, hence, for the convergence of the zeros. Thus, the number of nodes along

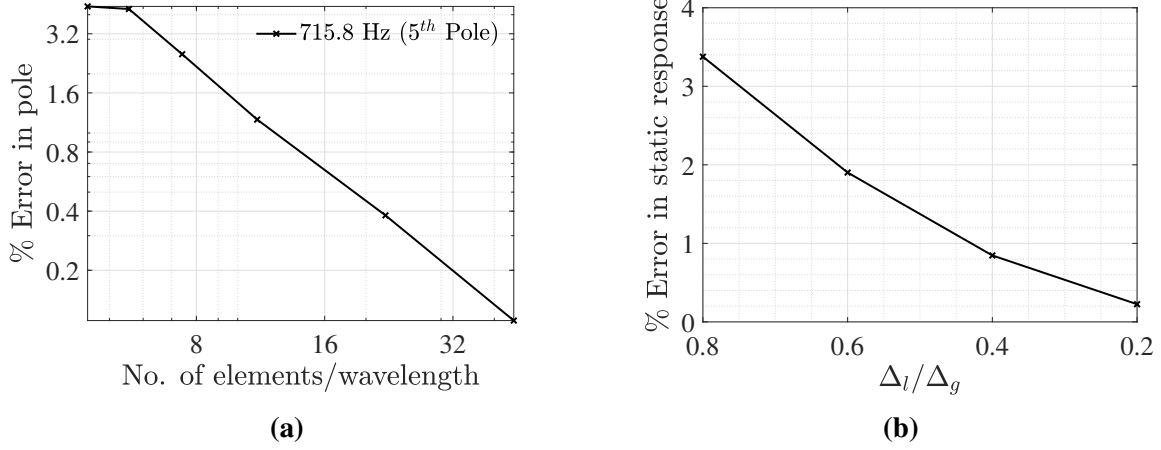


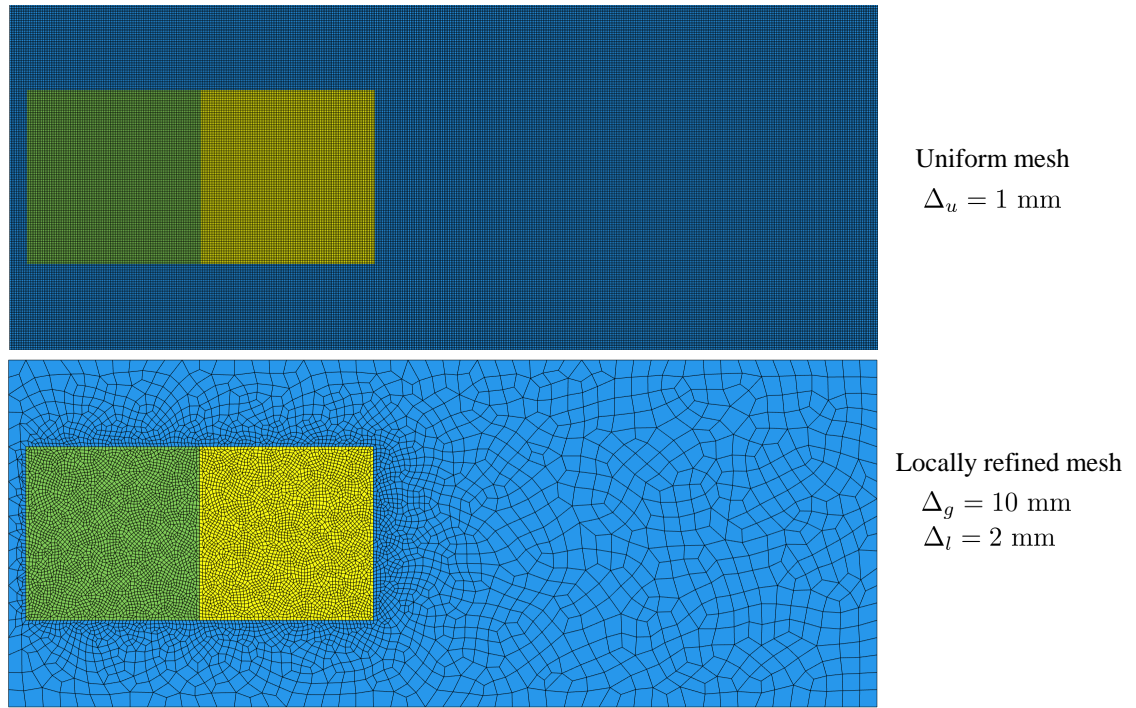
Fig. 20. (a) The global mesh convergence for the fifth pole and (b) local mesh convergence for static response in the case of cantilever plate equipped with non-collocated piezoelectric SA patches (Case-1NC)

the length of the patches (n_x) and the width of the patches (n_y) can be determined, respectively, as $n_x = p_L/\Delta_l + 1 = 100/2 + 1 = 51$ and $n_y = p_w/\Delta_l + 1 = 100/2 + 1 = 51$. The locally refined mesh has 9067 nodes \times 6 mechanical DOFs + 2 electrical DOFs. The uniform mesh and locally refined mesh and the corresponding FRFs are compared in Fig. 21. It is noted that the locally refined mesh produces almost the same converged FRF as the one produced by the uniform mesh. However, the locally refined mesh takes around 35 seconds which is only 13.4% of the total time taken by the uniform mesh.

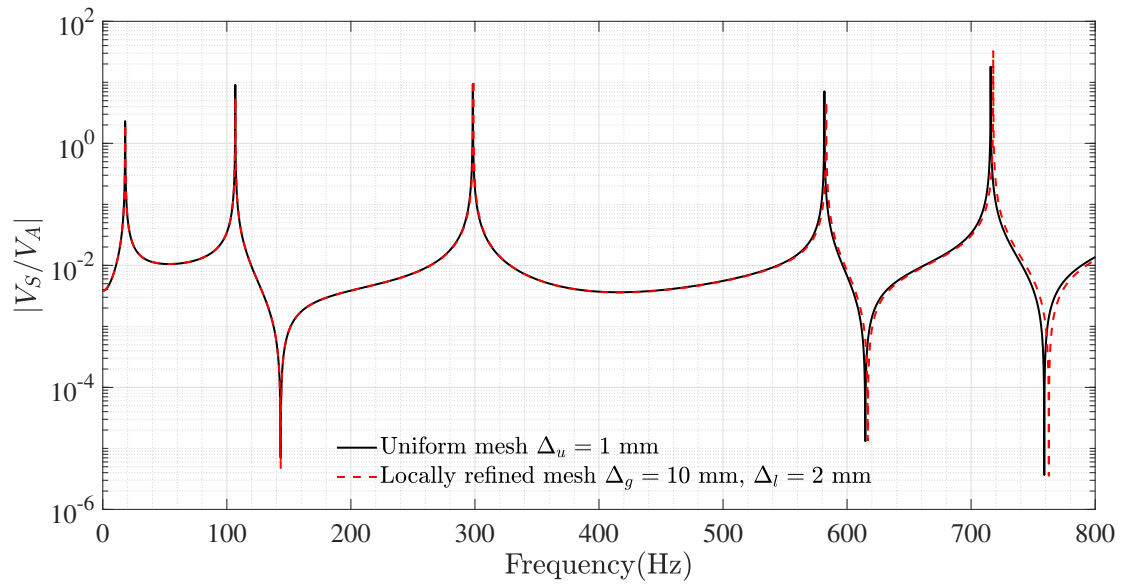
6 Physical Interpretation of Pole-Zero Pattern

An alternating pole-zero pattern is the most sought-after characteristic in the open loop FRF of a lightly damped structure for designing a robust and stable control system. The physical understanding of the poles and zeros is of immense help in deciding the sensor-actuator configuration to obtain the desired pole-zero pattern.

The poles of a system are physically represented by the natural vibration modes of the host-structure. On the other hand, the physical interpretation of the transmission zeros requires an in-depth understanding of the SA configuration. The transmission zeros of a force-displacement SA pair can be physically interpreted as the poles of the corresponding constrained system (Preumont, 2018). Since incorporating an extra constraint in the system increases the stiff-



(a)



(b)

Fig. 21. (a) The finite element models of the cantilever plate equipped with non-collocated piezoelectric SA patches with 1 mm uniform mesh size and with locally refined mesh, and (b) a comparison of the FRFs obtained using the two meshes

ness, therefore, the transmission zeros, in the case of force-displacement SA pair, appear at higher frequencies than the corresponding poles. Thus, a lightly damped system coupled with collocated force-displacement SA pair exhibits interlacing pole-zero pattern (starting with a pole). Similarly, in the case of a self-sensing single piezoelectric patch, the transmission zeros (of admittance) can be interpreted as the poles of the system when the electrodes are open (Preumont, 2006). The stiffness of a piezoelectric structure, in open-circuit, is higher than the short-circuit case due to which an alternating pole-zero pattern (starting with a pole) is observed. However, for a non-collocated system, as seen in Fig. 21(b), the pole-zero pattern may not remain interlaced and the pole-zero flipping may occur. Interestingly, in the case of a non-collocated force-displacement SA pair, it can be shown that the alternating pole-zero pattern remains preserved, at lower frequencies, if the sensor and actuator are closely spaced (Martin, 1978).

The previous discussions in this paper illustrated that the transmission zeros of a piezoelectric structure are closely connected with the static response. Therefore, a more detailed analysis is carried out in this section to develop a physical interpretation of the pole-zero pattern of piezoelectric structures in terms of static response of the system. Using the definition of transmission zeros (i.e., $G_{as}(\omega) = 0$) and the Eq. 8, the transmission zeros satisfy the following equation:

$$|D_M(\omega)| = |R(\omega)| \approx |S_M| \quad [\text{with opposite phase}] \quad (13)$$

To understand whether the pole-zero pattern starts with a pole or a zero, let us consider the first mode, i.e., $M = 1$. Thus, Eq. 13 can be rewritten as:

$$|D_1(\omega)| = |R(\omega)| \approx |S_1| \quad (14)$$

Hence, the first transmission zero appears when the contribution of the first mode $D_1(\omega)$ is equal to the static correction (or residual term) in magnitude but with opposite sign.

6.1 Collocated piezoelectric patches (*zero-after-pole*)

For the illustration, consider the example of the cantilever plate equipped with collocated patches (Case-1C). Since the dynamic response of the first mode D_1 does not include the correction for truncated modes, a static correction is applied to achieve the correct static response $G_{as}(0)(= D_1(0) + S_1)$ as shown in Fig. 22 (a). It is noticed that the static correction matches well with the residual term upto around 60 Hz (i.e., around 3 times of the first pole) because the modes are far separated as shown in Fig. 9. Therefore, the contribution D_1 of the first mode can be corrected for model truncation just by adding the static correction S_1 . This correction leads to the accurate static response and the first zero appears at 22.9 Hz as shown in Fig. 22 (b). As demonstrated in Fig. 8 (a), the actuator and sensor patches are subjected to the same curvature which leads to same sign of strain in the static response. Therefore, the sensor and actuator are in-phase in the static response (Fig. 22 (c)) and, hence, the sign of the static response is positive. Further, Fig. 22 (a) clearly shows that the magnitude of the static response is higher than $D_1(0)$. Therefore, the static correction S_1 must be of the same sign as that of $D_1(0)$ to ensure that: $S_1 + D_1(0) = G_{as}(0)$. The initial phase of the first mode is the same as that of the static response which changes after the first pole (Fig. 22 c) due to which the sign of D_1 also changes after the pole and becomes negative. Due to this sign change, the static correction S_1 cancels the D_1 at 22.9 Hz (intersection of the two curves in Fig. 22 b) where the first transmission zero appears. Thus, in this case the zero appears after the pole. Similarly, the formation of higher order zeros can also be explained following the above discussion. For example, Fig. 23 demonstrates the appearance of the second transmission zero at 125 Hz. It may be noted that in this case $M = 2$ in Eq. 13, therefore, D_2 represents the contribution of the first two modes and $S_2 + D_2(0) = G_{as}(0)$.

Moreover, this is a (nearly) collocated system, therefore, an alternating pole-zero pattern is observed (within the frequency ranges of interest) which starts with a pole as shown previously in Fig. 9.

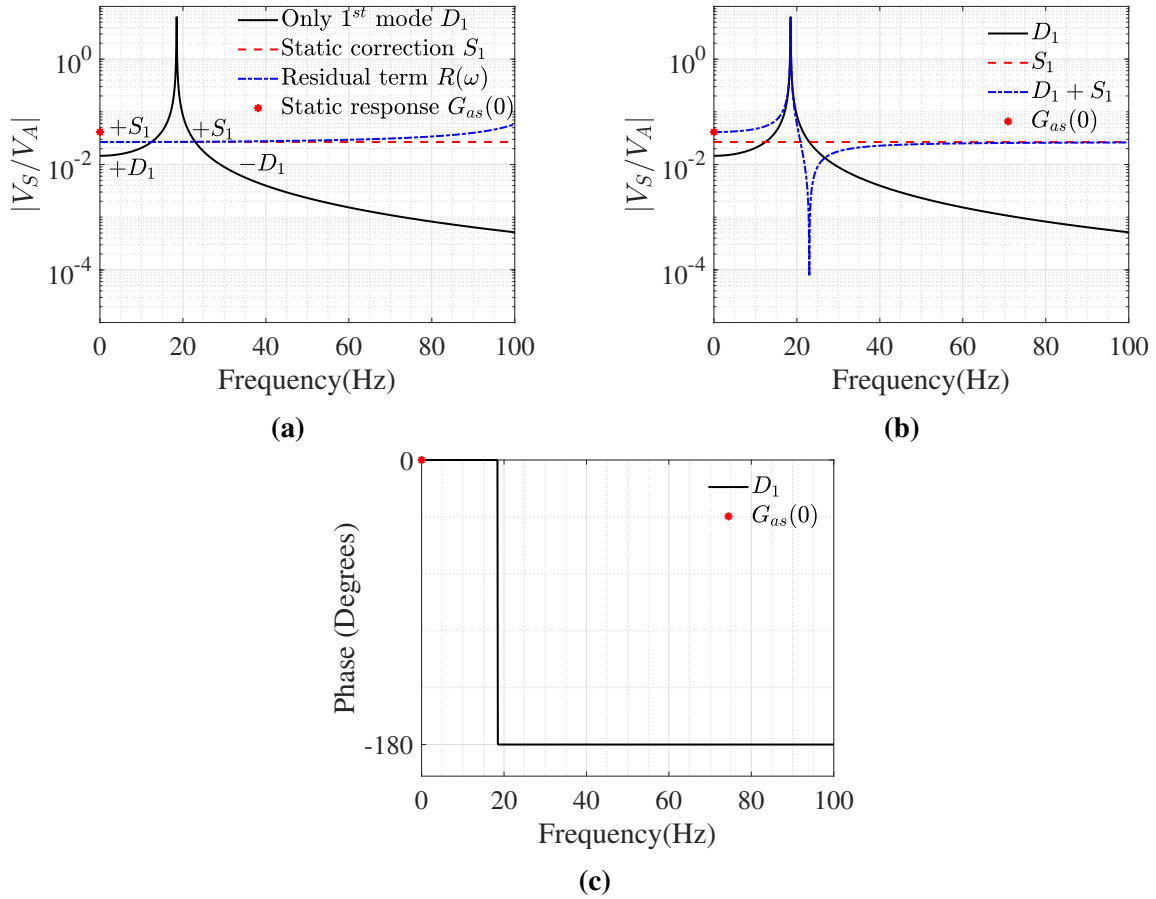


Fig. 22. (a) The contribution of the first mode in the FRF (D_1), (b) appearance of the first transmission zero after including the static correction (S_1) in the contribution of the first mode, (c) phase diagram of the first mode in the case of cantilever plate equipped with collocated patches (Case-1C)

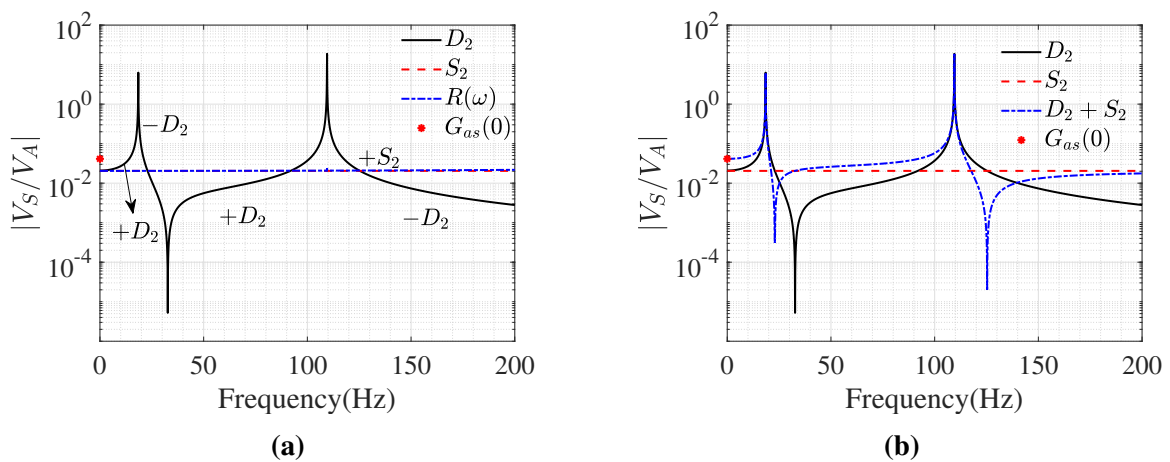


Fig. 23. (a) The contribution of the first two modes in the FRF (D_2), and (b) appearance of the second transmission zero after including the static correction (S_2) in the case of cantilever plate equipped with collocated patches (Case-1C)

Similarly, the ‘zero-after-pole’ situation is observed in the cases of clamped-clamped (Case-2C) and all-clamped plate (Case-3C) equipped with collocated patches that can be explained as shown in Fig. 24. Additionally, it is noted that in the case of all-clamped plate, the residual term $R(\omega)$ deviates significantly from the static correction term S_1 beyond 400 Hz due to closely spaced modes (Fig. 24 d). Therefore, the correct zero frequency is predicted by the intersection of the D_1 with $R(\omega)$ instead of D_1 with S_1 (Fig. 24 c). It may be noted that $R(\omega)$ quantitatively improves the value of the transmission zero but does not interchange the pole-zero pattern, as will also be seen in other examples in this study.

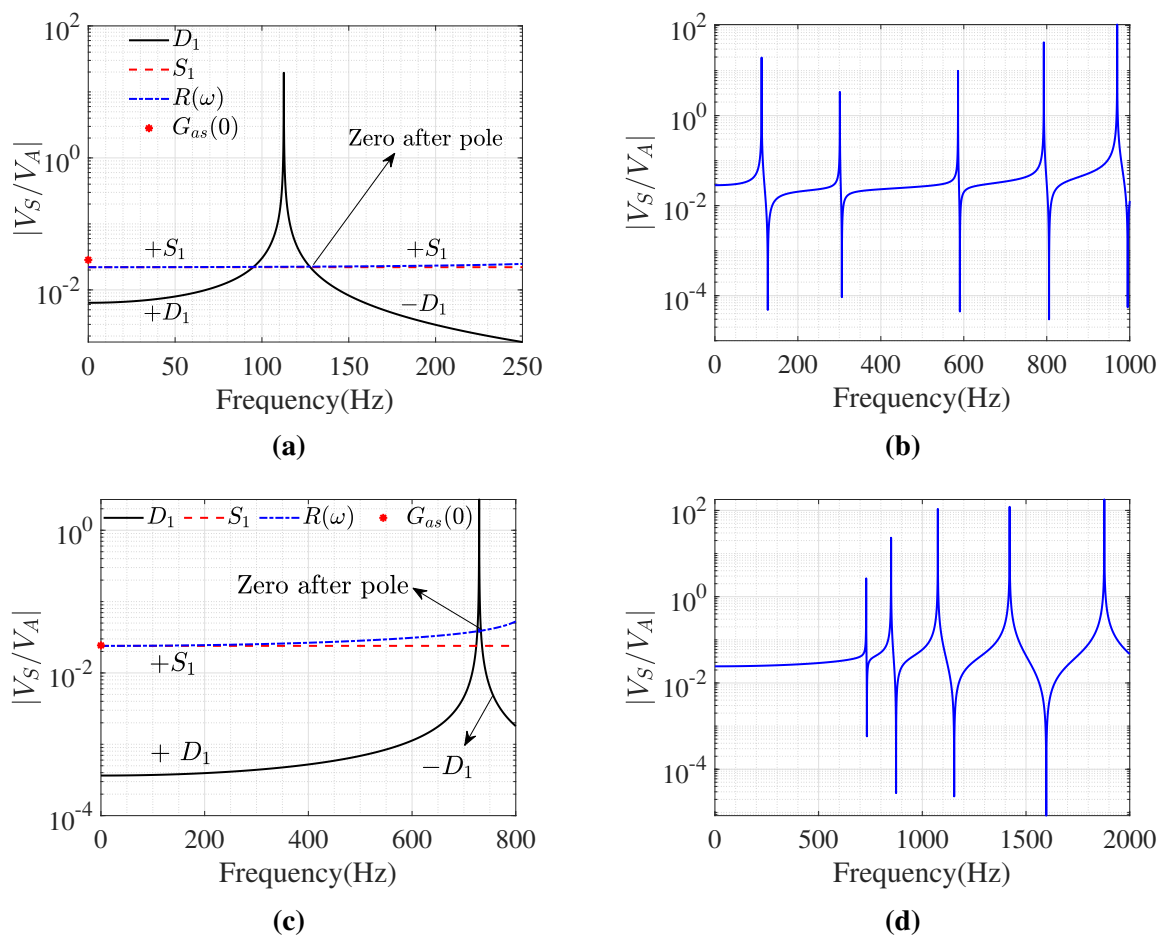


Fig. 24. An explanation of zero-after-pole situation and the full FRF depicting the pole-zero pattern, respectively, in the case of clamped-clamped plate (a,b) (Case-2C) and all-clamped plate (c,d) (Case-3C) equipped with collocated piezoelectric SA patches

6.2 Non-located piezoelectric patches (*no-zero case*)

In the example of the cantilever plate equipped with non-located patches (Case-1NC), the sensor and actuator patches are out-of-phase due to the different curvatures (Fig. 8 b). This leads to the negative sign of $G_{as}(0)$ and $D_1(0)$. Since $|G_{as}(0)| < |D_1(0)|$ (Fig. 25 a), therefore, the sign of S_1 should be opposite of $D_1(0)$ (i.e., positive). Thus, there is a possibility of zero appearing before the pole in this case. However, S_1 does not intersect D_1 and therefore, zero does not appear (Fig. 25 a). Moreover, the pole-zero pattern is not interlaced due to non-located patches (Fig. 25b).

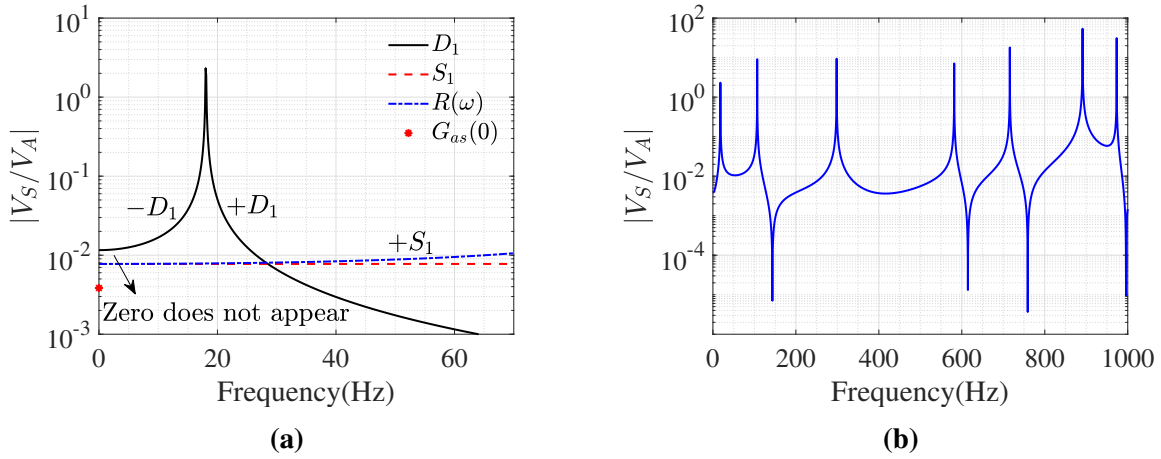


Fig. 25. (a) An explanation of ‘no-zero’ situation and (b) the full FRF depicting the pole-zero pattern in the case of cantilever plate equipped with non-located piezoelectric SA patches (Case-1NC)

6.3 Non-located piezoelectric patches (*zero-after-pole*)

In the case of clamped-clamped plate with non-located patches (Case-2NC), it is difficult to visualize the curvature difference between the SA patches in the static deflected shape due to the additional curvature effects introduced by the additional constraint (Fig. 26 a). In view of this, a detailed phase analysis is carried out which shows that $G_{as}(0)$ and $D_1(0)$ do not have any initial phase lag (Fig. 26 b). Based on this phase diagram, one may follow the previous discussions to explain the pole-zero pattern that starts with a pole in the present case as shown in Fig. 27.

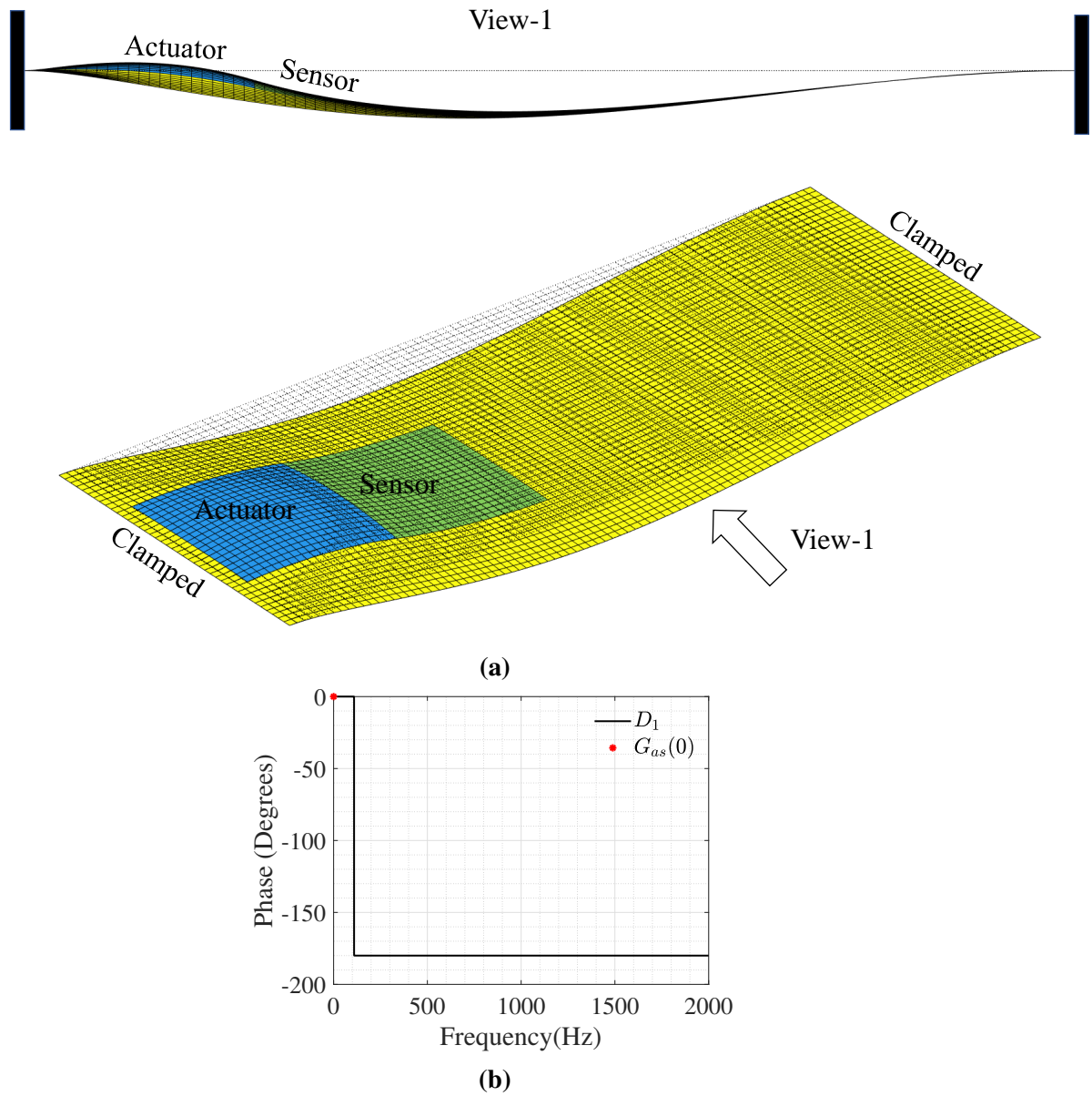


Fig. 26. (a) The static deflected shape and (b) phase diagram of the first mode in the case of clamped-clamped plate equipped with non-collocated piezoelectric SA patches (Case-2NC)

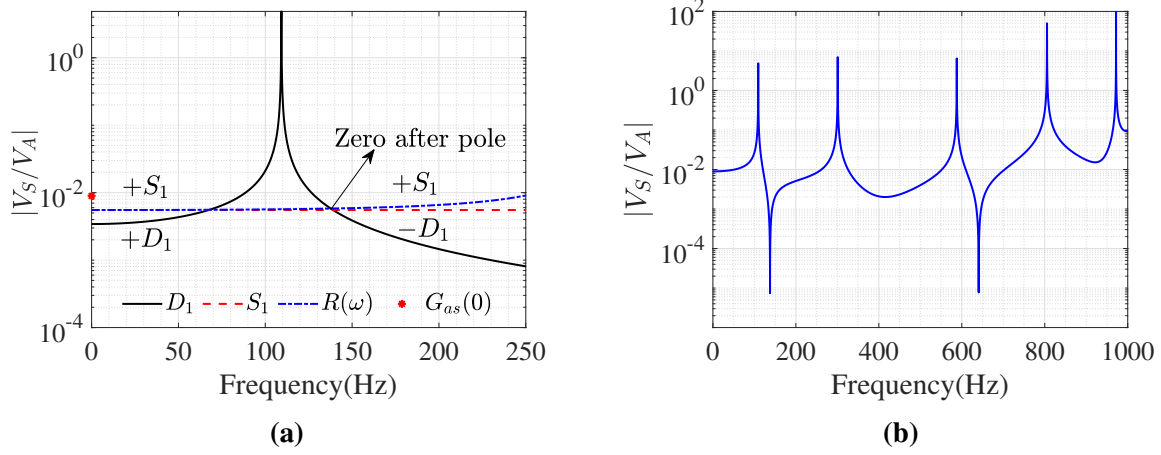


Fig. 27. (a) An explanation of ‘zero-after-pole’ situation, and (b) the full FRF depicting the pole-zero pattern in the case of clamped-clamped plate equipped with non-located piezoelectric SA patches (Case-2NC)

6.4 Non-located piezoelectric patches (*zero-before-pole*)

Now consider the case when all the edges of the plate are clamped (Case-3NC) for which the static deflected shape is shown in Fig. 28a. The major complication in the all-clamped plate is that it exhibits double curvature. By looking at view 1 and 2 in Fig. 28a, it seems that the actuator and sensor patches have nearly the same curvature in both the directions. Therefore, this suggests an initial zero phase lag in the static response as shown in Fig. 28 (b). On the contrary, there is an initial phase lag of 180 degrees in D_1 which causes the negative sign of D_1 . Although $|G_{as}(0)| > |D_1(0)|$ (Fig. 29 a), the sign of $G_{as}(0)$ is positive (opposite of $D_1(0)$). Therefore, S_1 should have a positive sign so that $D_1(0) + S_1 = G_{as}(0)$. Thus, in this case, the zero appears before the pole as shown in Fig. 29. In addition to this, the accurate position of zero is decided by the intersection of $R(\omega)$ with D_1 because, near the first transmission zero, the approximation $S_1 \approx R(\omega)$ does not remain valid due to the contribution of the closely-spaced modes (Fig. 29 b).

All the six cases considered here demonstrate that: (i) in the case of collocated patches, the zero appears after the pole which can be physically interpreted through respective static deflected shapes, (ii) in the non-located case, the physical interpretation becomes complex because the boundary conditions remarkably influence the curvature difference between the patch locations.

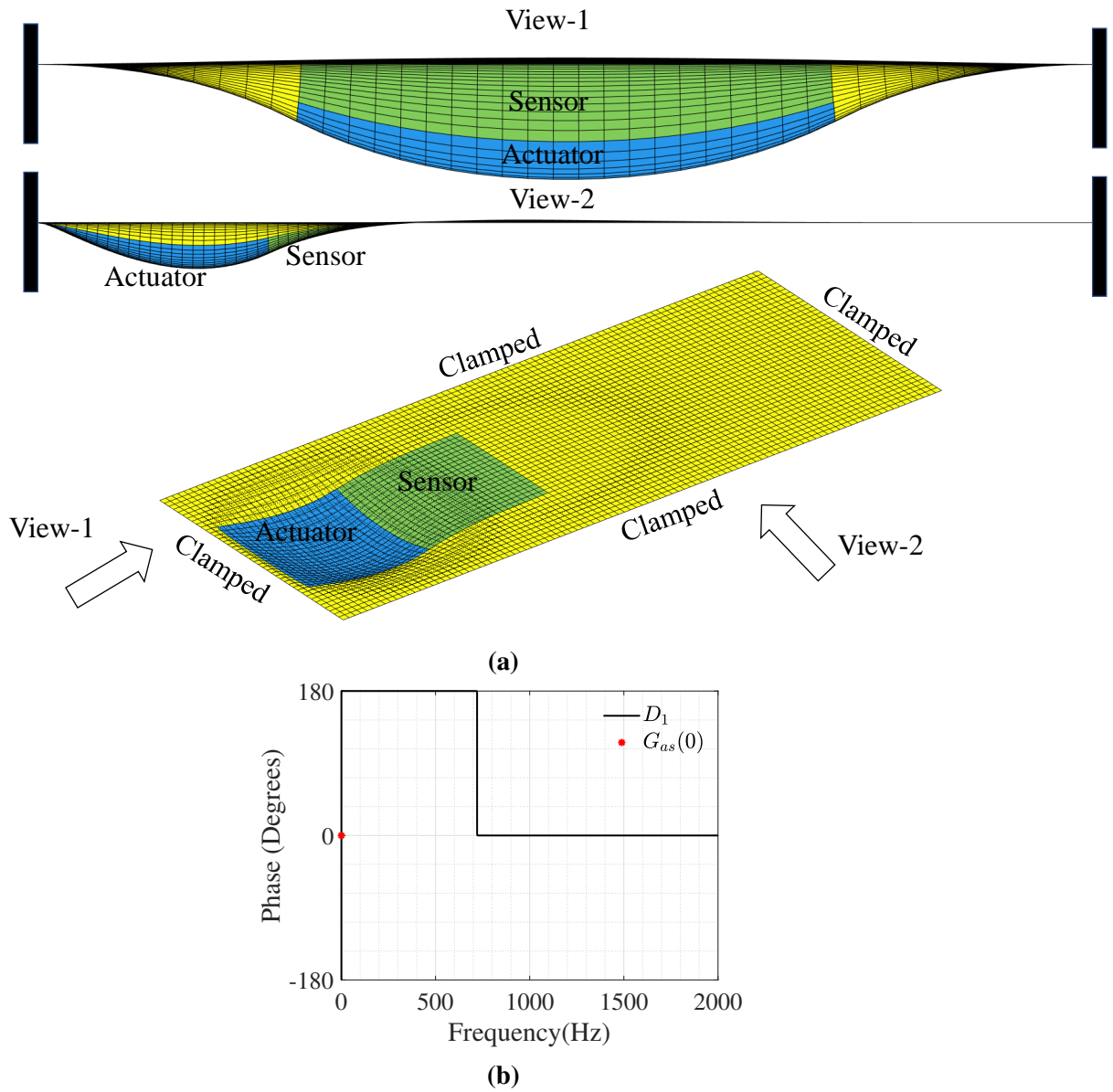


Fig. 28. (a) The static deflected shape and (b) phase diagram of the first mode in the case of all-clamped plate equipped with non-collocated piezoelectric SA patches (Case-3NC)

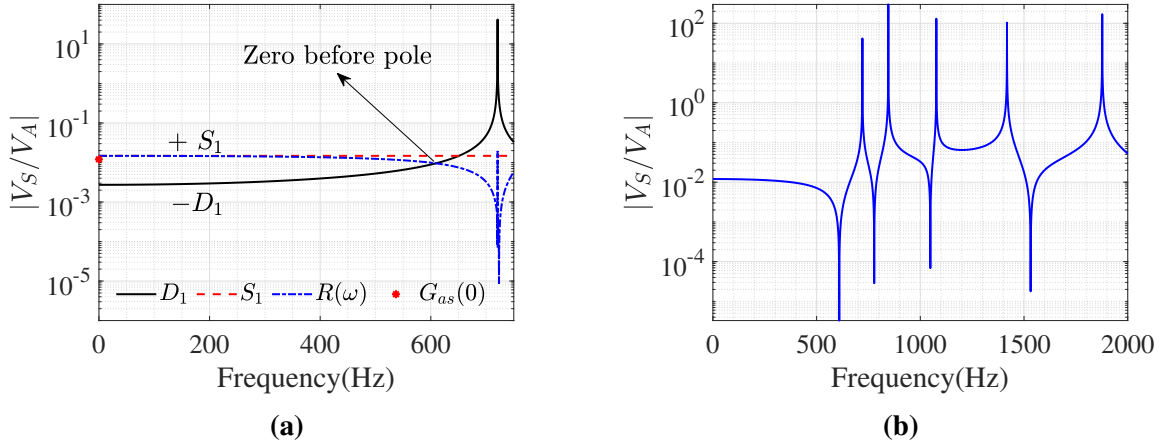


Fig. 29. (a) The explanation of ‘zero-before-pole’ situation, and (d) the full FRF depicting the pole-zero pattern in the case of all-clamped plate equipped with non-collocated piezoelectric SA patches (Case-3NC)

6.5 Influence of patch dimensions, locations, and orientation

Based on the above analysis, it is apparent that the pole-zero pattern of the piezoelectric structures can be altered to satisfy the design requirements by appropriately choosing the combinations of the size and the location of the patches. For example: if the previous example of all-clamped plate with non-collocated piezoelectric patches is changed by shortening the patch length to 20 mm and the patch location to 20 mm (Fig. 30a), then because of this smaller patch length both the patches have nearly the same curvature (Fig. 30a). In this case, the initial sign of D_1 also becomes positive and the zero appears after the pole (Figs. 30 b and c). Also, it is interesting to note that by reducing the length of the patches, the centroids of the two patches also come closer leading to a reduced degree of non-collocation. In addition to this, the approximation $R(\omega) \approx S_1$ remains valid in this case despite the fact that the modes are closely-spaced. This is possibly due to the negligible contribution of higher modes (notice the flat portion of the FRF curve between 1st and 2nd pole in Fig. 30 c). Similarly, changing the orientation of the patches can also affect the pole-zero pattern. To demonstrate this phenomenon, the orientation of the patches is changed orthogonally in the previous example and the corresponding static deformed shape is shown in Fig. 31(a). It is clearly observed that though the patches are smaller in size, still there is a noticeable difference in the curvature at the patch locations. This leads to a change of pole-zero pattern with zero appearing before the pole as shown in Figs. 31 (b) and (c).

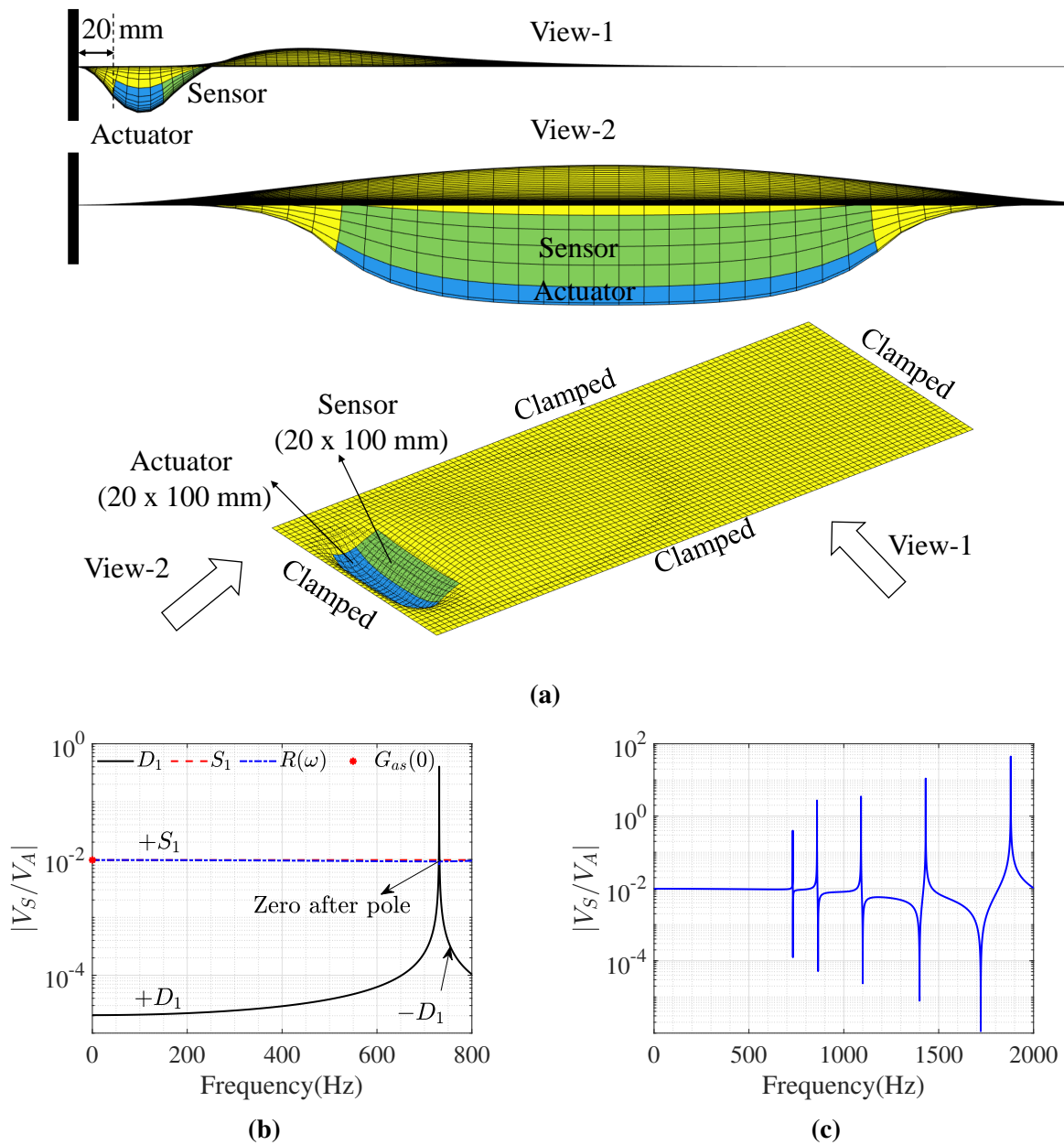


Fig. 30. (a) The static deflected shape, (b) the explanation of ‘zero-after-pole’ situation, and (c) the full FRF depicting the pole-zero pattern in the case of all-clamped plate equipped with non-collocated SA patches (20×100 mm)

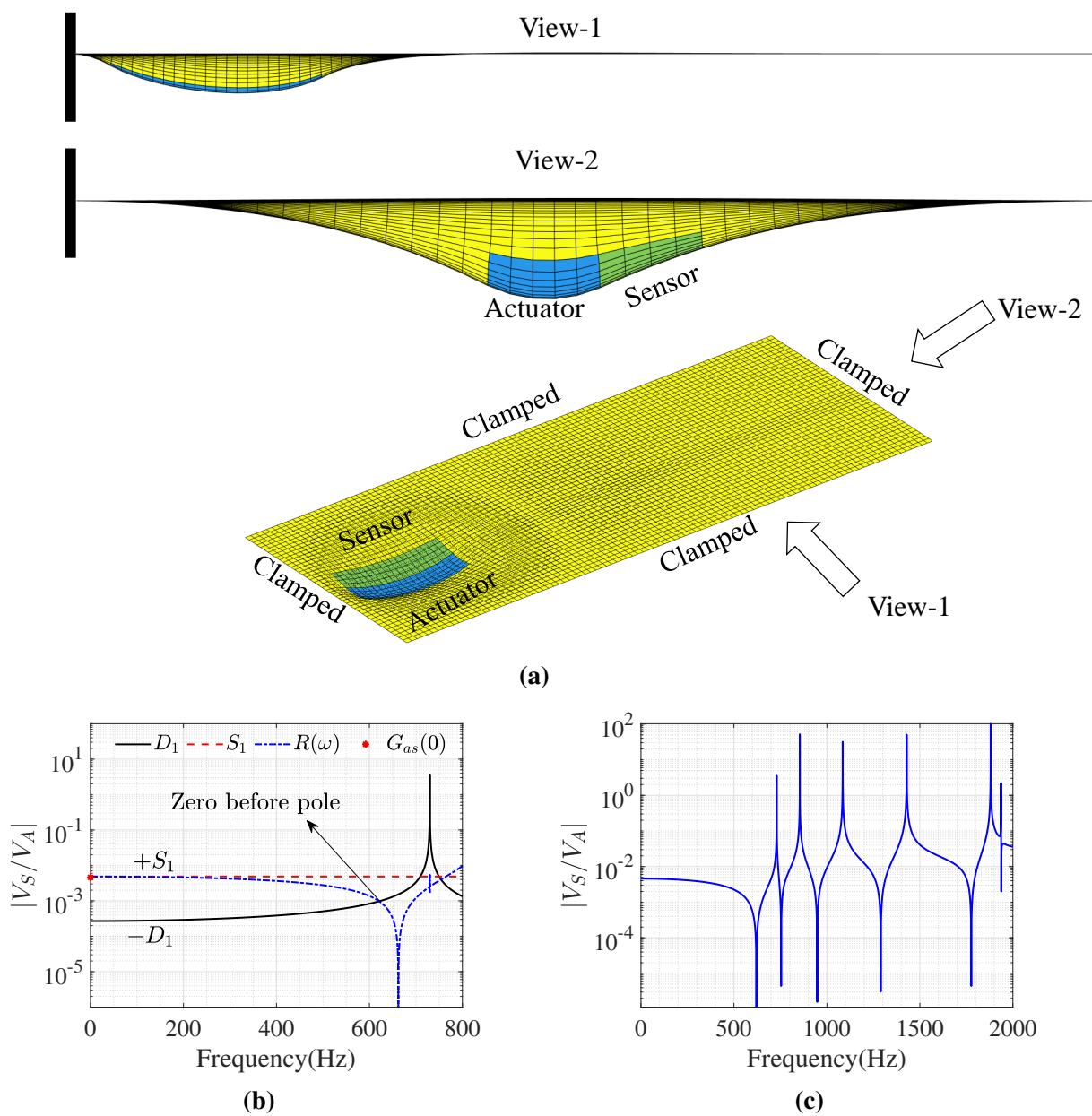


Fig. 31. (a) The static deflected shape, (b) the explanation of ‘zero-before-pole’ situation, and (c) the full FRF depicting the pole-zero pattern in the case of all-clamped plate equipped with non-collocated SA patches (20×100 mm) such that 100 mm dimension is oriented along the length of the plate

7 Conclusions

The evaluation of transmission zeros of the structures equipped with piezoelectric patches usually requires finite element modelling supplemented by model reduction. In this study, various combinations of boundary conditions (clamped, clamped-clamped, and all-clamped) and two configurations of the piezoelectric patches (collocated and non-collocated) are analyzed to demonstrate the effects of model truncation and model discretization on the evaluation of the transmission zeros of a thin rectangular plate equipped with a single pair of piezoelectric voltage sensor/ voltage actuator. These detailed investigations led to the following findings:

- The errors due to model truncation are much more significant in the case of piezoelectric structures compared to force-displacement pair(s) due to the local curvature induced by the piezoelectric actuator in the static deflected shape.
- The convergence of the transmission zeros depends on the convergence of the poles as well as the static response.
 - The pole-convergence is governed by the number of elements per bending wavelength of the mode of interest which explains the slower convergence in the case of higher modes and highly constrained structures.
 - The convergence of the static response depends on the accurate representation of the local curvature at the patch locations which explains the slower convergence in the case of non-collocated patches where the sensor and actuator patches are subjected to different curvatures.

Based on these findings, the first original contribution of this paper is the development of a numerically efficient local mesh refinement strategy. In this strategy, the global mesh size is governed by the pole convergence and the local refinement is carried out, at the patch location, by converging the static response. The merit of the locally refined mesh is demonstrated through an example of the cantilever plate equipped with non-collocated patches where a significant reduction in the computation time (around 85%) is observed for obtaining the converged zeros.

The second original contribution is to give a physical interpretation of the pole-zero pattern which states that:

- in the case of collocated patches the pole-zero pattern starts with a pole irrespective of the boundary conditions as there is no curvature difference between the sensor and actuator patches in the static response,
- for non-collocated patches where the sensor and actuator patches are subjected to the different curvatures, the pole-zero pattern may start either with a pole or with a zero depending upon the boundary conditions, location, size, and orientation of the patches.

The physical interpretation presented in this study can be explored further for more complicated structures such as rings, curved shells, and other periodic structures. Moreover, the physical interpretation given in this paper is an interesting tool to study alternative arrangements of piezoelectric patches in terms of location, shape, size and directivity which would enhance the performance of active control and can be the subject of further research.

Acknowledgement

This research has been funded by the ARC consolidator research program (project: IMpaCT, Integrated Mechatronics for Active vibration Control), Université Libre de Bruxelles, Brussels, Belgium.

References

- Alberts, T., & Colvin, J. (1991). Observations on the nature of transfer functions for control of piezoelectric laminates. *Journal of intelligent material systems and structures*, 2(4), 528–541.
- Allen, J., & Lauffer, J. (1992). Truncation effects on control design models. In *Proceedings of the 31st IEEE conference on decision and control* (pp. 1821–1823).
- Andersson, A., & Crawley, E. (1996). Transfer function shaping using distributed actuator-sensor pairs. In *Adaptive structures forum* (p. 1267).
- Balamurugan, V., & Narayanan, S. (2001). Active vibration control of smart shells using distributed piezoelectric sensors and actuators. *Smart Materials and Structures*, 10(2), 173.
- Balmes, E., & Deraemaeker, A. (2013). Modeling structures with piezoelectric materials. *SDT tutorial*.

- Bendine, K., Boukhoulda, B. F., Nouari, M., & Satla, Z. (2017). Structural modeling and active vibration control of smart fgm plate through ansys. *International Journal of Computational Methods*, 14(04), 1750042.
- Bendine, K., Boukhoulda, F., Haddag, B., & Nouari, M. (2019). Active vibration control of composite plate with optimal placement of piezoelectric patches. *Mechanics of Advanced Materials and Structures*, 26(4), 341–349.
- Besselink, B., Tabak, U., Lutowska, A., van de Wouw, N., Nijmeijer, H., Rixen, D. J., . . . Schilders, W. (2013). A comparison of model reduction techniques from structural dynamics, numerical mathematics and systems and control. *Journal of Sound and Vibration*, 332(19), 4403–4422.
- Bona, B., Calafiore, G., Carabelli, S., & Tonoli, A. (1996). Computation and physical interpretation of multivariate transmission zeros for lumped parameters colocated systems. *IFAC Proceedings Volumes*, 29(1), 4434–4439.
- Calafiore, G. (1997). A subsystems characterization of the zero modes for flexible mechanical structures. In *Proceedings of the 36th IEEE conference on decision and control* (Vol. 2, pp. 1375–1380).
- Calafiore, G., Carabelli, S., & Bona, B. (1997). Structural interpretation of transmission zeros for matrix second-order systems. *Automatica*, 33(4), 745–748.
- Chee, C. Y., Tong, L., & Steven, G. P. (1998). A review on the modelling of piezoelectric sensors and actuators incorporated in intelligent structures. *Journal of Intelligent Material Systems and Structures*, 9(1), 3–19.
- Clark, R. L., Fuller, C. R., & Wicks, A. (1991). Characterization of multiple piezoelectric actuators for structural excitation. *The Journal of the Acoustical Society of America*, 90(1), 346–357.
- Craig, R. R., & Bampton, M. C. (1968). Coupling of substructures for dynamic analyses. *AIAA journal*, 6(7), 1313–1319.
- Cudney, H., Alberts, T., & Colvin, J. (1992). A classical approach to structural control with piezoelectrics. In *33rd structures, structural dynamics and materials conference* (p. 2462).
- Davison, E., & Wang, S. (1974). Properties and calculation of transmission zeros of linear multivariable systems. *Automatica*, 10(6), 643–658.
- Dosch, J. J., Inman, D. J., & Garcia, E. (1992). A self-sensing piezoelectric actuator for colocated control. *Journal of Intelligent material systems and Structures*, 3(1), 166–185.
- Emami-Naeini, A., & Van Dooren, P. (1982). Computation of zeros of linear multivariable systems. *Automatica*, 18(4), 415–430.

- Fleming, F. M. (1990). *The effect of structure, actuator, and sensor on the zeroes of controlled structures* (Unpublished doctoral dissertation). Massachusetts Institute of Technology.
- Fleming, F. M., & Crawley, E. (1991). The zeroes of controlled structures-sensor/actuator attributes and structural modelling. In *32nd structures, structural dynamics, and materials conference* (p. 984).
- Geuzaine, C., & Remacle, J.-F. (2009). Gmsh: A 3-d finite element mesh generator with built-in pre-and post-processing facilities. *International journal for numerical methods in engineering*, *79*(11), 1309–1331.
- Grimme, E. (1997). Krylov projection methods for model reduction. *Ph. D. Thesis, University of Illinois at Urbana-Champaign*.
- Gripp, J., & Rade, D. (2018). Vibration and noise control using shunted piezoelectric transducers: A review. *Mechanical Systems and Signal Processing*, *112*, 359–383.
- Gupta, V., Sharma, M., & Thakur, N. (2010). Optimization criteria for optimal placement of piezoelectric sensors and actuators on a smart structure: a technical review. *Journal of Intelligent Material Systems and Structures*, *21*(12), 1227–1243.
- Halim, D., & Moheimani, S. R. (2003). An optimization approach to optimal placement of collocated piezoelectric actuators and sensors on a thin plate. *Mechatronics*, *13*(1), 27–47.
- Hariri, H., Bernard, Y., & Razek, A. (2015). Dual piezoelectric beam robot: The effect of piezoelectric patches' positions. *Journal of Intelligent Material Systems and Structures*, *26*(18), 2577–2590.
- Henrich, E. A., Gillis, J. T., & O'Connor, J. M. (1994). Spurious nonminimum phase zeros in models of smart structures. In *Smart structures and materials 1994: Smart structures and intelligent systems* (Vol. 2190, pp. 696–704).
- Iorga, L., Baruh, H., & Ursu, I. (2008). A review of h robust control of piezoelectric smart structures. *Applied Mechanics Reviews*, *61*(4).
- Lin, J. L. (1999). On transmission zeros of mass-dashpot-sepring systems. *Transactions of ASME, Journal of Dynamic Systems, Measurement, and Control*, *121*, 179–183.
- Lindner, D. K., Reichard, K. M., & Tarkenton, L. M. (1993). Zeros of modal models of flexible structures. *IEEE Transactions on automatic control*, *38*(9), 1384–1388.
- Martin, G. D. (1978). *On the control of flexible mechanical systems*. Department of Electrical Engineering, Stanford University.
- McCain, A. J. (1995). *Shaped actuators and sensors for local control of intelligent structures* (Unpublished doctoral dissertation). Massachusetts Institute of Technology.

- Miu, D. (1991). Physical interpretation of transfer function zeros for simple control systems with mechanical flexibilities. *Journal of Dynamic Systems, Measurement, and Control*, *113*, 419.
- Moghaddam, S. M. F., & Ahmadi, H. (2020). Active vibration control of truncated conical shell under harmonic excitation using piezoelectric actuator. *Thin-Walled Structures*, *151*, 106642.
- Moheimani, S. R. (1999). Experimental verification of the corrected transfer function of a piezoelectric laminate beam. In *1999 information, decision and control. data and information fusion symposium, signal processing and communications symposium and decision and control symposium. proceedings (cat. no. 99ex251)* (pp. 525–530).
- Moheimani, S. R., & Clark, R. L. (2000). Minimizing the truncation error in assumed modes models of structures. *J. Vib. Acoust.*, *122*(3), 332–335.
- Moheimani, S. R., & Fleming, A. J. (2006). *Piezoelectric transducers for vibration control and damping*. Springer Science & Business Media.
- Piefort, V. (2001). *Finite element modeling of piezoelectric active structures* (Unpublished doctoral dissertation). Ph. D. thesis. Bruxelles, Belgium: Université Libre de Bruxelles.
- Piefort, V., & Preumont, A. (2001). Modeling of smart piezoelectric shell structures with finite elements. In *Proceedings of the international seminar on modal analysis* (Vol. 2, pp. 869–876).
- Piron, D., Pathak, S., Deraemaeker, A., & Collette, C. (2021). A pole-zero based criterion for optimal placement of collocated sensor-actuator pair. *Mechanical Systems and Signal Processing*, *155*, 107533.
- Preumont, A. (2006). *Mechatronics: Dynamics of electromechanical and piezoelectric systems*. Springer.
- Preumont, A. (2018). *Vibration control of active structures: an introduction* (Vol. 246). Springer.
- Preumont, A., De Marneffe, B., & Krenk, S. (2008). Transmission zeros in structural control with collocated multi-input/multi-output pairs. *Journal of guidance, control, and dynamics*, *31*(2), 428–432.
- Qing, G., Qiu, J., & Liu, Y. (2006). A semi-analytical solution for static and dynamic analysis of plates with piezoelectric patches. *International journal of solids and structures*, *43*(6), 1388–1403.
- Qureshi, E. M., Shen, X., & Chen, J. (2014). Vibration control laws via shunted piezoelectric transducers: A review. *International Journal of Aeronautical and Space Sciences*, *15*(1), 1–19.
- Rao, S. S. (2007). *Vibration of continuous systems* (Vol. 464). Wiley Online Library.

- Rao, S. S., & Sunar, M. (1994). Piezoelectricity and its use in disturbance sensing and control of flexible structures: A survey. *Applied Mechanics Reviews*, 47(4), 113–123.
- Sharma, S., Kumar, A., Kumar, R., Talha, M., & Vaish, R. (2020). Active vibration control of smart structure using poling tuned piezoelectric material. *Journal of Intelligent Material Systems and Structures*, 1045389X20917456.
- Shivashankar, P., & Gopalakrishnan, S. (2020). Review on the use of piezoelectric materials for active vibration, noise, and flow control. *Smart Materials and Structures*, 29(5), 053001.
- Song, G., Sethi, V., & Li, H.-N. (2006). Vibration control of civil structures using piezoceramic smart materials: A review. *Engineering Structures*, 28(11), 1513–1524.
- Spector, V., & Flashner, H. (1990). Modeling and design implications of noncollocated control in flexible systems. *Journal of dynamic systems, measurement, and control*, 112(2), 186–193.
- Spier, C., Bruch, J., Sloss, J., Sadek, I., & Adali, S. (2011). Effect of vibration control on the frequencies of a cantilever beam with non-collocated piezo sensor and actuator. *IET control theory & applications*, 5(15), 1740–1747.
- Takács, G., et al. (2012). Mpc implementation for vibration control. In *Model predictive vibration control* (pp. 361–389). Springer.
- Tang, J., & Wang, K.-W. (2001). Active-passive hybrid piezoelectric networks for vibration control: comparisons and improvement. *Smart Materials and Structures*, 10(4), 794.
- Timoshenko, S. P., & Woinowsky-Krieger, S. (1959). *Theory of plates and shells*. McGraw-hill.
- Tondreau, G., Raman, S., & Deraemaeker, A. (2014). Point load actuation on plate structures based on triangular piezoelectric patches. *Smart Structures and Systems*, 13(4), 547–565.
- Van de Straete, H. J. (1995). *Physical meaning of zeros and transmission zeros from bond graph models* (Unpublished doctoral dissertation). Massachusetts Institute of Technology.
- Van de Straete, H. J., & Youcef-Toumi, K. (1996). Physical meaning of zeros and transmission zeros from bond graph models. *IFAC Proceedings Volumes*, 29(1), 4422–4427.
- Williams, T. (1989). Transmission-zero bounds for large space structures, with applications. *Journal of Guidance, Control, and Dynamics*, 12(1), 33–38.
- Williams, T. (1992a). Constrained modes in control theory: transmission zeros of uniform beams. *Journal of sound and vibration*, 156(1), 170–177.
- Williams, T. (1992b). Model order effects on the transmission zeros of flexible space structures. *Journal of guidance, control, and dynamics*, 15(2), 540–543.
- Williams, T. (1992c). Transmission zeros of non-collocated flexible structures-finite-dimensional effects. In *Dynamics specialists conference* (p. 2116).

- Wilson, E. L., Yuan, M.-W., & Dickens, J. M. (1982). Dynamic analysis by direct superposition of ritz vectors. *Earthquake Engineering & Structural Dynamics*, 10(6), 813–821.
- Wolovich, W. (1973). On determining the zeros of state-space systems. *IEEE Transactions on Automatic Control*, 18(5), 542–544.
- Xu, S., & Koko, T. (2004). Finite element analysis and design of actively controlled piezoelectric smart structures. *Finite elements in analysis and design*, 40(3), 241–262.
- Yang, J. (2005). *An introduction to the theory of piezoelectricity* (Vol. 9). Springer.